Geophysical Journal International

Seismicity in a model governed by competing frictional weakening and healing mechanisms

Journal:	*Geophysical Journal International*
Manuscript ID:	draft
Manuscript Type:	Research Paper
Date Submitted by the Author:	n/a
Complete List of Authors:	Hillers, Gregor; University of California, Santa Barbara, Institute for Crustal Studies Archuleta, R.J.; University of California, Santa Barbara, Institute for Crustal Studies Carlson, J.; University of California, Santa Barbara, Department of Physics
Keywords:	Fault zone rheology < COMPOSITION and PHYSICAL PROPERTIES, Friction < COMPOSITION and PHYSICAL PROPERTIES, Seismic cycle < GEODESY and GRAVITY, Rheology and friction of fault zones < SEISMOLOGY, Dynamics and mechanics of faulting < TECTONOPHYSICS

submitted to *Phys. Earth. Planet. Int.*

Seismicity in a Model Governed by Competing Frictional Weakening and Healing Mechanisms

G. Hillers[1], J. M. Carlson[2] & R. J. Archuleta[1,3]

[1]*Institute for Crustal Studies, University of California, Santa Barbara, California, 93106, USA*

[2]*Department of Physics, University of California, Santa Barbara, California, 93106, USA*

[3]*Department of Earth Sciences, University of California, Santa Barbara, California, 93106, USA*

SUMMARY

Observations from laboratory, field, and numerical work spanning a wide range of space and time scales suggest a strain dependent progressive evolution of material properties that control the stability of earthquake faults. The associated weakening mechanisms are counterbalanced by a variety of restrengthening mechanisms. The efficiency of the healing processes depends on local crustal properties such as temperature and hydraulic conditions. We investigate the relative effects of these competing nonlinear feedbacks on seismogenesis in the context of evolving frictional properties, using a mechanical earthquake model that is governed by slip weakening friction. Weakening and strengthening mechanisms are parameterized by the evolution of the frictional control variable—the slip weakening rate R—using empirical relationships obtained from laboratory experiments. Weakening depends on the slip of a model earthquake and tends to increase R, following the behavior of real and simulated frictional interfaces. Healing causes R to decrease and depends on the time passed since the last slip. Results from models with these competing feedbacks are compared with simulations using non-evolving friction. Compared to fixed R conditions, evolving properties result in a significantly increased variability in

the system dynamics. We find that for a given set of weakening parameters the resulting seismicity patterns are sensitive to details of the restrengthening process, such as the healing rate b and a lower cutoff time, t_c, up to which no significant change in the friction parameter is observed. For relatively large and small cutoff times, the statistics are typical of fixed large and small R values, respectively. However, a wide range of intermediate values leads to significant fluctuations in the internal energy levels. The frequency-size statistics of earthquake occurrence show corresponding nonstationary characteristics on times scales over which negligible fluctuations are observed in the fixed-R case. The progressive evolution implies that—except for extreme weakening and healing rates—faults and fault networks possibly are not well characterized by steady states on typical catalog time scales, thus highlighting the essential role of memory and history dependence in seismogenesis. The results suggest that an extrapolation to future seismicity occurrence based on temporally limited data may be misleading due to variability in seismicity patterns associated with competing mechanisms that affect fault stability.

Key words: Rheology and friction of fault zones—Dynamics and mechanics of faulting—Earthquake dynamics

1 INTRODUCTION

Faults evolve, organize, and interact in a fault network to accommodate relative plate motion. During this complex strain organizing process (Wesnousky 1988, 1999) the micro- and macromechanical properties of the involved materials constantly change, as crustal rocks are continuously deformed, transported, and altered as they are exposed to cyclic stresses and stress fluctuations associated with the earthquake cycle and remote earthquakes. Consequently, the friction coevolves in response to abrasive mechanisms, wear, progressive structural regularization and fluid assisted healing and restrengthening.

A number of laboratory and numerical experiments designed to isolate frictional rock properties suggest a transition from overall strengthening to weakening with continued deformation. In principle, an ensemble of relatively young, spatially distributed faults with rough sliding interfaces filled with unconsolidated gouge coalesces into simpler structures with ground interfaces hosting consolidated abrasive material. Friction associated with irregular sliding surfaces during initial breakup exhibits strengthening which is characterized by a relatively large fracture energy, G, required to create new

fracture surface or to break prominent surface irregularities. In the seismogenic part of the crust, frictional strengthening may be a result of dilatancy or local entropic effects (effective temperature) of granular aggregates, and is thus a typical response of less consolidated wear products (Marone 1998a; Langer 2008, and references therein).

Tectonically driven rock grinding processes, i.e., abrasion of contact asperities and continuous grain comminution, lead to the gradual development of fault zone gouge layers (Chester & Chester 1998; Chester et al. 2004). The properties of gouge layers govern the evolution of the frictional resistance during dynamic instabilities and therefore the behavior of earthquake faults (e.g., Scholz 1990; Chambon et al. 2006; Daub & Carlson 2008). The response of structurally simpler, relatively smooth faults with consolidated wear products is typically characterized by slip or velocity weakening, associated with smaller G values. Under these conditions, the frictional resistance drops to relatively low dynamic sliding levels, thus promoting the occurrence and propagation of large earthquakes.

The evolution of frictional properties reflects the organization of crustal and fault zone material (Ben-Zion & Sammis 2003). Dynamic friction is therefore sensitive to variable internal and external conditions, such as gouge characteristics and mechanical properties of the adjacent crustal material (see the Appendix for a more complete discussion). The interrelations of internal and external factors acting over broad spatiotemporal scales govern local coseismic weakening and interseismic restrengthening. Friction evolution is therefore a system response (Marone 1998b), rather than a locally isolated process.

Deformation induced weakening and counteracting time dependent healing thus alter the dynamic friction response. This suggests that from one earthquake to the next, friction may not be well described by a fixed function, even in a given location on a given fault. A fault system may not reach a steady state on time scales of few earthquake cycles, a consequence of the superposition of competing processes that influence the properties and stability of earthquake faults.

Acknowledging the poor constraints on in situ weakening and healing rates, we explore the effects of strength degradation and recovery in the context of evolving frictional properties, using a slip weakening friction law. The friction law is defined by the material strength F_0, the weakening rate R, and the residual sliding level f_s (Fig. 1a). Conceptually, the level of f_s relative to the stress or force outside the hypocentral area at the onset of an instability influences the dynamic response and thus the slip pattern of an earthquake. Because R controls the slip $\Delta u = d_c$ necessary to reach f_s, it governs the overall friction behavior and seismic response. We incorporate history dependence through variation of the weakening rate R with slip and time and contrast it with the fixed-R case.

Although time and history dependence is an important aspect of the rate-and-state laws, the framework does not account for the evolution of friction over long time scales and the corresponding evolution

of parameters that control stability, e.g., the frictional slip rate dependence (Ruina 1983). Using the rate-and-state framework in multi-cycle simulations, the healing controls the repetitive restrengthening after model earthquakes, but healing does not affect the dynamic regime which does not change for a given set of parameters and boundary conditions. For rate-and-state, it also less clear how to construct a comparison study with a scenario of evolving properties such as the slip rate dependence or the critical slip distance.

To explore long term effects of friction evolution efficiently we choose a one-dimensional mechanical model, i.e., a Burridge-Knopoff representation of an earthquake fault as shown in Figure 1(b) (Burridge & Knopoff 1967; Carlson & Langer 1989a). The model is governed by the slip weakening law shown in Figure 1(a) and formally introduced in Section 3 (Eq. 7). Evolution of the weakening rate R parameterizes changes in dynamic friction. Together, the primitive representation of a lateral fault and the linear slip weakening friction represent the most abstract level to investigate long term consequences of evolving friction parameters.

We focus on heterogeneity associated with dynamics as opposed to intrinsic material heterogeneity. Increasing and decreasing values of R correspond to transitions from relatively strong to weak conditions and vice versa. The dependence of R on slip and interevent hold time follows empirical relationships that describe phenomena observed at different spatiotemporal scales (Sec. 2). While previous numerical experiments mostly explored time independent friction parameters, we investigate consequences of feedbacks, friction evolution, and resulting seismicity patterns. Throughout this study, the term 'feedback' is associated with slip and time dependent changes of the control variable R, as opposed to elastic force interactions or the 'positive feedback' that drives accelerating failure processes (Sammis & Sornette 2002).

Section 2 presents observations related to strength degradation and healing, and describes how the observations are parameterized in our friction model. Section 3 introduces the numerical implementation, and in Section 4 we compare the results for systems with fixed vs. evolving friction. We conclude with a discussion of the implications of our results for observed seismicity. The Appendix discusses in more detail additional phenomena affecting the mechanical properties of rocks and the friction behavior of a fault and thus its seismicity.

2 WEAKENING AND STRENGTHENING PROCESSES

2.1 Weakening

The weakening of bulk properties such as the degradation of rigidity, and the change of frictional resistance governing the mechanical behavior of sliding surfaces, depends on the deformation history.

The strain dependence is deduced from observations on different scales, which suggest a progressive coevolution of micro- and macroscopic fault characteristics. On the microscopic end, laboratory experiments that measure the decrease of the friction breakdown distance d_c (Marone & Kilgore 1993) and the increase of gouge volume (Wang & Scholz 1994), and numerical experiments on synthetic gouge thickness (Guo & Morgan 2007) show a qualitatively similar dependence on shear displacement. On the macroscopic end, field measurements of geometric fault trace heterogeneity indicate a progressive regularization of structural complexity as a function of cumulative fault offset (Wesnousky 1988). Together, these studies indicate an initially fast decrease of d_c for gouge filled surfaces, a high initial wear rate of rough surfaces, a fast increase of gouge thickness during early stages of deformation, and a rapid initial decrease of fault irregularities. The initial fast rates are consistently followed by a more gradual change at relatively larger displacements, where details depend on external variables, e.g., normal stress.

Wang & Scholz (1994) expressed this collective behavior in a relationship describing the gouge volume as a function of slip. Supported by the qualitatively similar behavior of smoothing processes observed under various conditions, we approximate changes of the dynamic control variable R (the slip weakening rate, Fig. 1a) due to displacement using (Wang & Scholz 1994)

$$\Delta R^w = \left(\gamma_0 + A\frac{k_2}{k_1}\right)\left(1 - e^{-k_1 \Delta u}\right) + k_2 A \Delta u. \quad (1)$$

Equation 1 describes the changes in R due to weakening ('w') as a function of slip, Δu. Here, γ_0 is the initial gouge volume, and A is a measure of the contact area. In our analysis γ_0 and A will not be used explicitly, but are used to scale the range of ΔR^w to appropriate values (Sec. 4.2.1). The wear coefficients $k_1 > 0$ and $k_2 \geq 0$ parameterize the efficiency of the wear process, and we will focus on the properties of the function controlled by k_1. For $k_2 = 0$, ΔR^w is proportional to $1 - e^{-k_1 \Delta u}$, where larger k_1 leads to a greater change at smaller Δu. That is, the initial slope of the function $\Delta R^w = \Delta R^w(\Delta u)$ as well as the transition between rapid and gradual increase of ΔR^w are controlled by k_1. For $k_2 > 0$, the sum in paranthesis scales the asymptote of the $1 - e^{-k_1 \Delta u}$ term, and the third term leads to a linear increase of ΔR^w beyond the rapid-to-gradual transitions. Note that the form of Equation 1 is compatible with the power-law approximation derived by Guo & Morgan (2007), suggesting a generic character for the evolution function.

2.2 Strengthening

Restrengthening is essential for stick slip and repetitive earthquakes on faults. This section discusses the mechanical and frictional properties that are affected by healing, how these observations are imple-

mented in our model, and the observed variability in the parameters that describe these mechanisms. Healing can be due to one or more mechanisms, such as contact yielding, compaction, fluid assisted changes in rheology associated with stress induced dissolution and redeposition, crack closure due to ductile creep, and chemical precipitation leading to cementation and crack sealing (Li et al. 2006, and references therein). These mechanisms affect mostly the strength of a frictional interface, which can be a fault that has slipped or microcracks whose density and distribution control bulk elastic properties. A general observation is that friction interfaces regain strength depending on the logarithm of contact or hold time, t_h (Dieterich & Kilgore 1994). This decreasing healing rate with time has been documented in laboratory experiments (Dieterich 1972, 1978). Observations of the recovery of seismic velocities after earthquakes, and source property changes from repeating earthquakes are compatible with this behavior (Vidale et al. 1994; Marone et al. 1995; Hickman & Wong 2001; Hiramatsu et al. 2005; Li et al. 2006).

In contrast to the $\ln(t_h)$ dependence, studies on pressure solution (Yasuhara et al. 2005), normal stress changes (Richardson & Marone 1999), and cohesive strengthening (Tenthorey & Cox 2006) imply a significantly faster-than-$\ln(t_h)$ healing, demonstrating the sensitivity of restrengthening mechanisms to variable conditions of a fault. Furthermore, healing rates may differ after two seemingly similar, 'characteristic' events, depending on details of the preceding rupture and the associated creation of fracture and flow networks.

Different strengthening mechanisms possibly affect different properties of a friction parameterization (Tenthorey & Cox 2006). Nakatani & Scholz (2004) found that the dynamic friction evolution distance d_c is also affected by changing conditions that cause a large variability in the cutoff time t_c. Furthermore, d_c correlates with the width of gouge zones and the roughness of sliding surfaces (Marone 1998a; Ohnaka 2003). For bare surfaces, the time dependent increase of contact junctions (Dieterich & Kilgore 1994) suggests that d_c—which is interpreted to be the slip that brings a new set of joints into contact—depends indirectly on time, too. For gouge filled surfaces, Marone & Kilgore (1993) found a deformation dependent reduction of d_c due to shear localization. Healing might then work against localization (Lyakhovsky et al. 1997a), associated with an increase in d_c, which is equivalent to an increase in the weakening rate R assuming a constant frictional sliding level (Fig. 1a). Thus in our model strengthening ('s') is implemented applying the widely observed logarithmic dependence on hold time to R,

$$\Delta R^s = -b \ln \left(\frac{t_h}{t_c} + 1 \right). \tag{2}$$

The $\ln(t_h)$ dependence, with t_h the time elapsed since the last slip on a fault, assumes a lower cutoff time, t_c, up to which no significant increase in state or strength is observed (Nakatani & Scholz 2006). Beyond t_c, healing shows a log-linear growth with slope b. The minus sign in Equation 2 stems from

the fact that stronger conditions (larger asperity contacts) are associated with smaller weakening rates (larger d_c). The values of b and t_c control the healing behavior, and we thus use b and t_c as tuning parameters for restrengthening processes. Nakatani & Scholz (2004) observed values for $b \approx 0.01$, in agreement with previously reported rates used in the rate-and-state theory (Dieterich 1978), while measurements of the cutoff time t_c vary over many orders of magnitude and depend strongly on temperature and hydraulic conditions.

The dry experiments conducted by Dieterich (1972) at room temperature indicate t_c is of the order of 0.1 to 1 sec for the laboratory system. However, these conditions neglect temperature dependent and fluid assisted processes at depths associated with nucleation regimes of large earthquakes (Scholz 1990). Nakatani & Scholz (2004) performed experiments that simulate a range of hydrothermal conditions and found an inverse dependence of t_c on temperature, measuring values between $t_c = 10^3$ sec and $t_c = 5 \times 10^4$ sec. Moreover, healing on natural faults suggests t_c may be as large as 9×10^6 sec (Marone et al. 1995). Nakatani & Scholz (2006) concluded that t_c is not an intrinsic constant of the healing process, and t_c may depend on the state immediately after a slip event.

Choosing different combinations of the weakening and healing parameters k_1, k_2 (Eq. 1), and b, t_c (Eq. 2), respectively, we investigate the properties of synthetic seismicity of a mechanical earthquake fault model discussed next.

3 SIMULATION STRATEGY

3.1 Numerical Implementation

We use a one-dimensional Burridge-Knopoff (Burridge & Knopoff 1967) model of a spring-slider chain connected to a loader plate moving with velocity v^∞ as shown in Figure 1(b) (Carlson & Langer 1989a,b; Carlson et al. 1991). The individual mass of the n blocks is m, the strength of the slider connecting springs is k_c, and k_p is the strength of the leaf springs between the loading substrate and each sliding element. The term F is the slip dependent friction law discussed below. With x_i denoting the displacement of block i measured from equilibrium position, the equations of motion for this system are (overdots represent time derivatives)

$$m\ddot{x}_i = k_c \left(x_{i+1} - 2x_i + x_{i-1}\right) - k_p v^\infty - F. \tag{3}$$

See Xia et al. (2005) for solution strategies. In Equation 3 the sum of the first and second term on the right hand side at a time t is the elastic force or stress acting on an element, $K_i(t)$. The average stress or strain energy in the system, which is dominated by the average position of the blocks with respect

to the position of the loader plate, is the normalized sum of $K_i(t)$ over all blocks,

$$E(t) = n^{-1} \sum_{i=1}^{n} K_i(t). \tag{4}$$

The corresponding standard deviation, a measure of stress or energy fluctuations associated with the variability of block spacings, is estimated using

$$\delta E(t) = \left[n^{-1} \sum_{i=1}^{n} (K_i(t) - E(t))^2 \right]^{1/2} \tag{5}$$

(Ben-Zion et al. 2003), and the temporal averages of these measurements are denoted as $\bar{E}$ and $\delta\bar{E}$, respectively. Values of E and δE are scaled respectively by the maximum possible internal energy, E^*, and a value corresponding to large fluctuations, δE^*. Inspection of Equation 3 reveals that E^* is identified with F_0, assuming a configuration at rest and equally spaced blocks. Recall that F_0 is the peak strength of the frictional interface. Similarly, δE^* is derived assuming a distribution of random block offsets x_i drawn from a uniform probability distribution in the interval $[0,\ 1]$. Such a configuration is extremely unlikely to occur during the evolution of the system, and not observed during our numerical experiments. The offsets are scaled to equilibrate the driving force and the frictional strength at the position where the k_c-term in Equation 3 is maximum. For the parameters given below $\delta E^* = 1.13$, found by averaging δE computed from 10^4 random block offset configurations.

Slip is measured in $u_i = x_i/D_0$, with $D_0 = F_0/k_p$, the maximum distance the loader plate can move before a block starts slipping. The characteristic loading time is $t^* = D_0/v^\infty$, i.e., the time required for the loader plate to move the maximum displacement before a block starts slipping. Constant parameters used throughout this study are $n = 5000$, $m = 1$, $k_p = 40$, $k_c = k_p l^2$, $l = 10$, $F_0 = 3$, $v^\infty = 10^{-9}$, and the dynamic time step during integration using a fourth order RK method (Press et al. 1992) is $\delta t = 0.001$. The size of an event is measured in the equivalent of seismic potency, the integral slip over the slipped area, which reduces to

$$P = \sum_{j \in I} \Delta u_j, \tag{6}$$

where I denotes the subset of blocks that slipped during an event. Consequently, P is measured in units of slip.

Previous studies focused on the model behavior as a function of the friction term F in Equation 3, and used different versions of a velocity weakening friction law. Here we use slip weakening friction of the form

$$F = \begin{cases} F_0 \left(\max \left[f_s, 1 - \sigma - R\,\Delta u \right] \right), & \text{if } \Delta u > 0 \text{ (block is slipping);} \\ (-\infty, F_0], & \text{if } \Delta u = 0 \text{ (block is at rest).} \end{cases} \tag{7}$$

Here, f_s is the frictional sliding level, $\sigma = 0.01$ approximates an infinitesimal drop in frictional resistance once the threshold F_0 is exceeded (Carlson et al. 1994), and R denotes the weakening rate, given in units of F_0 and D_0. That is, for $R = 1$, $\sigma = 0$, and $f_s = 0$ friction drops from $F = F_0$ to $F = 0$ over the distance $\Delta u = D_0$ (Fig. 1a).

In Section 4, we perform simulations using fixed, time independent R values, and later sections discuss slip and time dependent changes of the slip weakening rate. To apply the feedback rules in Equations 1 and 2, the weakening rate is adjusted as follows. Let t_1 and t_2 denote the times of two successive instabilities at position i. Then R_i^{1-} and R_i^{1+} denote R_i immediately before and after the instability at t_1, and R_i^{2-} is the value at the onset of slip at t_2. As discussed in Section 2.1, slip weakens an interface, and this weakening is parameterized by a slip dependent increase in R_i

$$R_i^{1+} = \min\left[R^u, R_i^{1-} + \Delta R_i^w\right], \tag{8}$$

where ΔR^w is sensitive to choices of k_1, k_2 (Eq. 1). That is, the amount ΔR^w is added to the value at the onset of the instability, R_i^{1-}, but the new value R_i^{1+} does not exceed the upper bound R^u. Note that the value of R_i is adjusted after the event, but the friction behavior of a block is governed by R_i^{1-}, and does not change during the event. At t_2, the onset of the next instability at position i, the time $t_h = t_2 - t_1$ is determined and R_i adjusted according to

$$R_i^{2-} = \max\left[R^l, R_i^{1+} + \Delta R_i^s\right], \tag{9}$$

where ΔR^s depends on b and t_c (Eq. 2). Recall that ΔR^s is negative, and the weakening rate thus decreases down to a minimum value R^l. The upper and lower bounds of the R range, R^u and R^l, are discussed in Section 4.1.1. We assume a separation of time scales, i.e., we assume a zero load velocity limit ($v^\infty = 0$ during instabilities) that prevents temporal overlap of consecutive but spatially separated events.

All discussed results consider data recorded after the initial transients. The system size has been taken to be sufficiently large that we avoid finite size effects. The ratio of the number of blocks involved in the largest events, n_I, to the system size, n, never exceeds $n_I/n = 0.45$, and in most cases is significantly smaller.

3.2 Dynamic Control Variables

Before we turn to simulation results (Sec. 4), we discuss the friction parameters F_0, R, and f_s. The frictional strength F_0 determines the maximum load an interface can sustain. Because of heterogeneous material properties of crustal rocks, and spatially variable restrengthening mechanisms (Sec. 2.2) the evolution of heterogeneous distributions of F_0 is physically plausible. For simplicity we ig-

nore this material source of heterogeneity in our model which would require a more elaborate scheme to determine t and i for the next nucleation. It would also lead to spatiotemporal changes in the characteristic distance $D_0 = F_0/k_p$, which would make it more difficult to identify the involved length and time scales appropriately. For reasons of computational simplicity we therefore refrain from changing F_0 as a function of slip or time and set $F_0 = const.$, and vary R and f_s.

In Section 4.1 we consider the behavior of the system in response to a range of fixed friction parameters R and f_s. First, we assume a constant frictional sliding level f_s. A large (small) weakening rate, R, corresponds to a small (large) fracture energy, G (Fig. 1a). Relatively large (small) values of R do (do not) allow F to drop to $F_0 f_s$ over the distance $\Delta u = d_c$, leading to effective weakening (strengthening). Recall that strengthening and weakening are associated with the dynamic response of unconsolidated, disorganized granular aggregates and solidified crustal material, respectively (Sec. 1). Second, we test the implications of a change in the residual sliding level, f_s, which controls the strength drop when F_0 and R are both held constant. Changes in f_s reflect the observation that the degree of surface roughness correlates with the steady state friction coefficient. That is, for a fixed R strengthening occurs more rapidly for larger values of f_s, which implies a reduced possibility of rupture propagation. The potential effect of variable f_s is indicated by the 3D studies of Zöller et al. (2005b) and Mehta et al. (2006), who use the strength drop as a heterogeneity and tuning parameter, respectively.

4 RESULTS

4.1 Time Invariant Homogeneous Frictional Conditions

4.1.1 Statistical Properties

This section quantifies how slip patterns and the corresponding frequency-size statistics change as a function of fixed homogeneous friction parameters R and f_s. Figure 2 shows slip evolution patterns in response to a constant frictional sliding level, $f_s = 0.5$, and variable weakening rates, R. The relatively large fracture energy G associated with a small weakening rate results in frictional strengthening, prohibiting accelerated, unstable slip (Fig. 2a). This is also reflected in significantly reduced slip rates during ruptures compared to instabilities governed by larger R values, and the events in Figure 2(a) have thus a creep-like character. Larger rates R lead to conditions that favor unstable slip (Figs 2b and c), because there is less dissipation. For intermediate values ($R = 1$), the system exhibits a broad range of event sizes, compared to large values ($R = 2$) for which the energy release is dominated by the occurrence of very large events.

The largest events for $R = 0.5$ involve approximately as many blocks as the large events for $R = 2$, and hence show the same delocalized character, but have two orders of magnitude less slip. The small

offsets imply a relatively regular block spacing, leading to approximately equally strained loader springs, and the forces K_i are close to the failure strength F_0. This synchronization is a result of low offsets during an unstable slip event, and is also reflected by the high internal energy level, E, discussed below. In the three cases shown in Figure 2, small events are confined to localized regions.

The system produces a wide range of event sizes, with the potency P spanning five orders of magnitude for $R = 0.5$, and the range increases for $R > 0.5$. Figures 3(a) to (d) show frequency-size statistics produced by systems with $f_s = 0.5$ and $R = [0.5,\ 1,\ 1.3,\ 2]$ (cf. Fig. 2). For values smaller than $R \approx 1$ friction does not drop to low residual levels during unstable slip, which suppresses the propagation of instabilities and the accumulation of coseismic slip. The corresponding seismicity distribution exhibits Gutenberg-Richter (GR) power-law scaling for small, localized events. The distribution is truncated by an exponential tail, indicating the lack of very large events (Figs 2a and b, 3a and b). In the earth, this feature is typically associated with structurally heterogeneous, immature stages of faulting (Wesnousky 1994; Stirling et al. 1996). As R increases in our simulations towards $R = 1$, the range of power law scaling also increases. For $R > 1$ a separate population of very large events develops (Figs 3c and d), leading to 'hybrid' statistics with energy release dominated by events of a characteristic size, reminiscent of natural seismicity of structurally simpler faults (e.g., Wesnousky 1988; Ben-Zion 1996; Hillers et al. 2007).

The transition from the power-law scaling with exponential cutoff to a characteristic earthquake (CE) distribution with excess large events is accompanied by (1) a reduction of the overall productivity (the 'a' value in the GR scaling $\log N = a - b \log P$, with N the number of events of size P), (2) an increased maximum event size, P^*, and (3) the widening of the gap between relatively small and (very) large event populations. The opposite trend of an increase in the productivity for $R = 1$ (Fig. 3b) compared to $R < 1$ (Fig. 3a) is explained by the occurrence of local stress concentrations in the vicinity of large, approximately Gaussian shaped slip events (Fig. 2b). In general, the results are consistent with statistical properties of seismicity produced by faults at different evolutionary stages, suggested by observational and numerical evidence (Wesnousky 1988; Ben-Zion 2008).

Comparing the properties of synthetic seismicity obtained with the slip weakening law (Eq. 7) to the corresponding results using velocity weakening friction verifies the importance of the weakening rate for the system dynamics (for velocity weakening friction the weakening rate α in Carlson & Langer 1989b; Carlson et al. 1991, 1994, plays a role similar to the slip weakening rate R in this paper). The R dependence of the event size $\tilde{P}$, which marks the approximate transition between small and large events, is compatible with the analysis in the Carlson et al. papers, where it was shown that the corresponding $\tilde{P}$ is a function of the weakening rate parameter α. Similarly, the saturation of P^*—it does not increase for $R > 2$—has been found to be independent of the friction response, controlled instead

by the elastic properties of the system (k_c, k_p, F_0).

Figure 4 illustrates the resulting frequency-size distributions as a function of the slip weakening rate, R, and the frictional sliding level, f_s, for a range of fixed values. The figure illustrates that the statistics are most sensitive to the weakening rate R. In the present model, the strength drop, $1 - f_s$, plays only a secondary role. The relative insensitivity to the range of f_s values considered here for $R < 1$ is explained by the small offsets Δu during 'slow slip' events, because the relatively small R values prevent the frictional resistance F from reaching the residual level f_s. From this point on we use R as the variable friction parameter in the limits $R^l = 0.5 \leq R \leq R^u = 2$ (Eqs 8 and 9), and keep $f_s = 0.5$ constant.

4.1.2 Energy Measurements

Energy measurements allow us to track the temporal evolution of the system dynamics. Figure 5 illustrates $E(t)$ and $\delta E(t)$ (Eqs 4 and 5) in two systems with small ($R = 0.5$) and large ($R = 2$) weakening rates, respectively. In addition to the original data plotted after each individual slip event (black), two temporally smoothed functions of $E(t)$ and $\delta E(t)$, $E_{dt}(t)$ and $\delta E_{dt}(t)$, are shown. They are average values of E and δE from consecutive time windows of length dt and overlap $dt/2$. The figure shows two cases: for $dt = t^*/2$ (red) and $dt = t^*/10$ (blue). Trivially, a smaller time window leads to functions that are similar to the originals, whereas functions averaged over larger windows approximate the long term averages, $\bar{E}$ and $\delta\bar{E}$.

The strain energy level $\bar{E} = 0.989$ is close to unity (the maximum value) for $R = 0.5$ (Fig. 5a) which indicates that the system is always strained to a very high degree, because of the inefficient weakening mechanisms associated with a small R. Conversely, the lower internal energy level in response to $R = 2$ ($\bar{E} = 0.65$) reflects the quasiperiodic occurrence of efficient energy releasing, large, delocalized events. The corresponding level of the energy fluctuations $\delta\bar{E} = 8 \times 10^{-3}$ (Fig. 5b) for low values of R are small, indicating a relatively homogeneous and synchronized system dynamics. The large amplitudes produced by the large-R model reflect significant energy changes caused by intermittent large slip events. Values around $\delta E = 0.45$ reflect a substantial degree of internal organization, compared to $\delta E = 1$ associated with random test configurations (Sec. 3.1).

Higher energies and smaller fluctuations are associated with stronger material properties, which prohibit the propagation of large cascading events. Correspondingly, the temporal averages $\bar{E}$ and $\delta\bar{E}$ indicate that smaller energy levels and larger fluctuations are associated with the quasicyclic occurrence of delocalized events. A progression from higher to lower average values of $\bar{E}$ and corresponding increases in $\delta\bar{E}$ is consistent with organization of fault zone material and corresponding friction evo-

lution. As a result, fault systems progressively increase the capability for an efficient strain energy release as we demonstrate in the next section.

Figure 6 summarizes the results of the time invariant, fixed conditions, in a E_{dt} vs. δE_{dt} plane, showing results for $dt = t^*/10$ (polygons) and $dt = t^*/2$ (colored circles). Smaller (larger) averaging time windows dt result in an increase (decrease) of the variability around the long term average, $\bar{E}, \delta\bar{E}$ (black circles). Conceptually, counterclockwise pathways from the lower right to the upper left reflect organization and regularization of a system, associated with improved efficiency in releasing accumulated strain energy through the production of large slip events. Opposite pathways in the E_{dt} vs. δE_{dt} plane are associated with higher strength and dissipation, and coincide with an increased occurrence of small events and a reduced probability of large events. We note that we do not observe consistently directed trajectories within datasets corresponding to particular choices of R and dt, which could indicate a coherent change or evolution of system dynamics. Rather, the patterns are consistent with undirected fluctuations around the mean.

4.2 Evolving Frictional Properties

4.2.1 Feedback Parameterization, Length and Time Scales

To implement the weakening and strengthening processes discussed in Section 2, it is useful to consider the relevant length and time scales. We begin this section with a discussion of the weakening length scales associated with observations introduced in Section 2.1. From this we infer a distance d_t that characterizes the transition from initial frictional strengthening to later weakening behavior.

In the laboratory experiments by Marone & Kilgore (1993), the initially large critical slip distance d_c reaches a lower, constant value for a shear strain of about 10, but the ratio between the initial and a later constant value depends on the gouge particle size distribution and layer thickness. In the Wang & Scholz (1994) rotary shear experiments, the change in wear rate from initially high values to reduced normal stress dependent steady state values occurs at about 10 cm. The numerical experiments by Guo & Morgan (2007) of strained particle ensembles indicate a change in plastic deformation from distributed to localized shear at a displacement of 10 mm. Note that these experiments do not simulate stick slip episodes, but continuous deformation; hence, the strains should not be confused with strains at which rocks fail in earthquakes ($\sim 0.1\%$). According to Marone (1998a), the microscopic distance d_t reflects the length scale of the stability transition associated with the discussed measurements at the microscopic scale (d_c, wear rate, and localization). Since laboratory measurements need to be scaled when applied to macroscopic scales, he argues that an upscaled value of d_t might be applied to the transition from fast to gradual change of geometric fault zone heterogeneity with increasing cumulative fault offsets (Wesnousky 1988).

Therefore, we rescale the the transition distance d_t associated with the discussed microscopic observations to approximate mechanisms at a larger scale. This is based on the conclusion that the breakdown distance d_c also depends on the observation scale, i.e., laboratory and field estimates of d_c differ by orders of magnitude (Perfettini et al. 2003). Given the uncertainties in the observations related to the stability transition, we make an estimate of the transition distance d_t using a scaling factor similar to the ratio of estimates of the microscopic to macroscopic critical slip distance (Bizzarri & Cocco 2003). Hence, the transition distance d_t in our model is equivalent to an offset $\Delta u = D_0$, assuming D_0 to be of the order of 1 to 10 m (Table 1).

Using Equation 1, this translates into a transformation of R from strong ($R = 0.5$) to weak ($R = 2$) conditions, restricting ΔR^w to lie between 0 and 1.5. Figures 7(a) and (b) display ΔR^w (Eq. 1), i.e., the increase of R as a function of slip for different sets of k_1 and k_2. Starting with an initial value of $R = 0.5$, different functions cross the boundary between weak and strong behavior associated with $R \approx 1$ (Fig. 4) and thus $\Delta R^w \approx 0.5$ at different fractions of D_0. Figure 7(b) illustrates that the evolution of a system is strongly controlled by the increase of R at small displacements in the initial small-R regime.

As discussed in Section 2.2, values for the healing parameter b are of the order of 0.01, and the cutoff time t_c has been observed to vary by several orders of magnitude. The time scale of seconds, associated with the duration of unstable slip episodes, is related to the slipping time of a single block in our model, $\omega_p^{-1} \propto k_p^{-1/2}$ (Carlson & Langer 1989b), and leads to a ratio of slipping time—synonymous to earthquake duration—to load time of about 2×10^{-9}. This proportion agrees with the ratio of the duration of seismic slip to interevent times of large earthquakes on real faults.

Figures 7(c) and (d) show the increment $\Delta R^s(t_h)$ and the evolution of R as a function of the time a block is at rest, t_h, $R(t_h) = R(t_h = 0) + \Delta R^s(t_h)$ (Eq. 2), for different values of the parameters b and t_c. Recall that the value of R at i is updated after an event terminates and at the onset of the next instability at i (Eqs 8 and 9). For values of $b = 0.01$ the time required for total healing ($\Delta R^s = -1.5$, $R = 2 \rightarrow 0.5$) barely counterbalances increases in R associated with maximum displacements of the order of D_0, with an approximate repeat time t^* ($R > 1$). However, the magnitude of maximum slip during instabilities in the initial small-R regime is much less than D_0, about $10^{-4} D_0 < \Delta u < 10^{-2} D_0$. According to Figure 7(b), slip of this magnitude increases R in the range of 0 to 0.3, depending on k_1 and k_2. Hence, a subsequent change of $-\Delta R^s$ of similar magnitude is necessary to reach the starting level $R = 0.5$, to keep the system in the strengthening regime. This illustrates the role of the parameters b and t_c in determining $-\Delta R^s\,(t_h)$, with t_h being a locally and temporally variable quantity.

Because the value of the macroscopic stability transition distance ($d_t = D_0$) is less well constrained

by data than direct measurements of b and t_c, we focus on results using one set of parameters $k_1 = 0.4$ and $k_2 = 0$. The implications of different choices will be separately discussed. Choosing $d_t = D_0$ leads to ranges of ΔR^w in the small-R regime that can be counterbalanced by $-\Delta R^s$ using $b = 0.01$, a value typically observed in experimental situations. We will use a fixed weakening parameterization, values around $b = 0.01$, together with systematic variations of t_c (Table 1). As demonstrated in the following sections, our numerical experiments cover a large range of system behavior without using extreme parameter choices, that illustrates the distinction between systems with fixed and evolving friction.

4.2.2 System Dynamics

Similar to Sections 4.1.1 and 4.1.2 we use frequency-size statistics and energy measurements to analyze the dynamics of systems with evolving friction. We contrast these results to our previous results for fixed friction parameters. We begin with the discussion of energy measurements, and conclude with examples of frequency-size statistics.

We set the parameters $k_1 = 0.04$ and $k_2 = 0$ (Figs 7a and b) which leads to a relatively rapid transition from stronger to weaker material properties, accompanied by large changes in R as a result of relatively small coseismic offsets Δu which occur in the small-R regime. Figure 8 displays measurements of E_{dt} and δE_{dt} for $b = 0.01$, $b = 0.02$ and variable cutoff times, t_c. All simulations start with $R = 0.5$. Data are recorded beginning at time $t = t^*$ after the initial transients have passed. The competing weakening and strengthening feedbacks start operating at $t = 2t^*$. Visual inspection of energy measurements indicate that the transients associated with the beginning of the feedbacks do not last longer than approximately $3t^*$ to $5t^*$. The discussion of system dynamics in response to evolving friction considers data unaffected by these transients ($t > 5t^*$).

In Figure 8(a) ($b = 0.01$), a small cutoff time $t_c \leq 10$ sec (grey, green data) keeps the system in the small-R regime. This is because healing starts with a very short delay and thus counterbalances slip dependent increases of R soon after an event terminates. However, compared to the 'small-R reference' results displayed in Figure (5) the $t_c \leq 10$ sec cases (Fig. 8) develop significant deviations of E_{dt} and δE_{dt} from the seemingly straight lines $E_{dt} = 0.989$ and $\delta E_{dt} = 8 \times 10^{-3}$. This indicates that the competition between weakening and strengthening influences the system dynamics, leading to intermittent conditions allowing large events to occur. Further reduction of the cutoff time t_c results in progressive suppression of the fluctuations. Systems with $t_c \geq 50$ sec exhibit dynamics corresponding to an overall weaker regime, indicated by smaller (larger) E_{dt} (δE_{dt}) levels. Figure 8(a) indicates that at the large end of the t_c range considered here (blue data), the healing induced increases of R, ΔR^s, are too small to effectively counterbalance weakening. Consequently, the energy measurements do not

differ significantly from the fixed 'large-R reference' case (Fig. 5). The responses to t_c in the range 10 to 100 sec (Fig. 8 red, black data) indicate that the respective systems show significantly larger fluctuations of E_{dt} on time scales of tens of loading cycles. Interestingly, the level of energy variations δE_{dt} are higher compared to the case $t_c = 10^3$ sec (blue data), which shows a lower E_{dt}. This illustrates that conditions in which weakening and strengthening conditions are roughly balanced produce the largest variability (fluctuations in E, level of δE) in the system dynamics.

A qualitatively similar response to increasing t_c is observed using $b = 0.02$ (Fig. 8b). The increased healing rate shifts the relevant range of t_c to larger values, $t_c = 2 \times 10^3$ to 20×10^3 sec, to obtain results similar to Figure 8(a) with $b = 0.01$. For the smallest $t_c = 10^3$ sec (grey data) considered here, the system dynamics are almost identical to the fixed-$R = 0.5$ case, i.e., healing dominates the response. Larger t_c (green, red, black data) results in energy measurements similar to the $b = 0.01$ case, showing a progressive decrease of the energy level E, fluctuations of E over time intervals which are long compared to the fixed-R simulations, and an increase in the energy variations δE at a given time. For the largest cutoff time, $t_c = 2 \times 10^4$ sec (blue data), weakening dominates and the dynamics are similar to the fixed-$R = 2$ case.

We performed additional simulations using different weakening curves (Eq. 1 with different values of k_1, k_2), indicated in Figure 7(a) (dashed lines). For a given coseismic offset Δu, a smaller value of ΔR^w, equivalent to less efficient weakening, requires a smaller healing rate or larger cutoff time to evolve towards weaker large-R conditions. A reduction of d_t to values smaller than D_0 (Figs 7a and b) together with larger healing rates or smaller cutoff times has a similar effect.

In summary, the results show that fast (slow) healing, parameterized by relatively large (small) healing rates and small (large) cutoff times, suppress (support) the development of persistent weakening properties. For a broad range of intermediate parameter values, we observe significant fluctuations in the energy measurements on time scales that are large compared to the time scales of fluctuations in response to non-evolving friction properties. Measurements of the energy level E show that a system can intermittently be in an overall weak state (small $E \leftrightarrow$ large R), whereas at later times the properties may exhibit strengthening characteristics (black data Fig. 8b around $t = 10t^*$ and $t = 24t^*$). Details such as the time associated with these transitions ($14t^*$) depend on the values for b and t_c, but the qualitative results are robust over a range of parameters that control the evolution of R. This suggests that fluctuations on time scales of multiple earthquake cycles may be a generic feature of an evolving threshold system with competing frictional weakening and strengthening.

Figure 9 displays the temporal behavior of the systems discussed in Figure 8 in the E_{dt} vs. δE_{dt} plane, showing typical evolution paths for different values of the weakening and healing rates. The trajectories depend on b and t_c, and except for limiting values the fluctuations—δE as well as the range of δE

and E—are large compared to the fixed-R cases (Fig. 6). The data indicate a transition from strengthening to weakening dynamics. Strengthening (weakening) dynamics are characterized by a high (low) energy level E, a large (small) variability of δE at a relatively low (high) δE level. The two dynamic regimes correlate with up-down trajectories in the lower right and left-right trajectories in the upper left of the E_{dt} vs. δE_{dt} plane. The results are sensitive to the time window dt, but are found to be robust for $dt \geq 0.5\,t^*$ (Fig. 9c). These illustrations confirm that efficient healing as a consequence of relatively small values of the cutoff time t_c does not allow a system to develop behavior corresponding to large-R conditions (see grey and green data in Figs 8 and 9). In these examples, periods of reduced energy E due to the occasional occurrence of large events increase the variability, indicated by significant changes in δE. However, the reductions in E are small, because the frictional properties of only a limited set of blocks I has undergone significant change. Because of the longer periods the involved sliding elements $i \in I$ are at rest, their R values heal back to the maximum strength. A qualitatively similar behavior is observed for larger cutoff times. Figure 9(d) expands a section of data from $10\,t^*$ (Fig. 8b, black data), sampling E_{dt} and δE_{dt} values with $dt = 0.5\,t^*$. Progressively darker shades of grey illustrate the temporal evolution, indicating a period of significant strengthening (clockwise pathway) followed by weakening (opposite trajectory). Though this type of pattern is consistently observed in the dynamics, we do not observe a systematic temporal pattern for the time ranges considered.

While the analysis of E and δE measurements permits a detailed analysis of our numerical simulations, the corresponding observations cannot be made on real faults. To discuss properties that are observable, we consider temporally variable properties of synthetic frequency-size statistics. Figure 10 shows three examples of frequency-size distributions from simulations with $b = 0.02$ (Fig. 8), where the corresponding subcatalogs contain seismicity for five consecutive time windows of duration $2t^*$, covering data from $t = 5t^*$ to $t = 15t^*$. Differences in seismicity rates for a given potency P in subsequent time windows vary for different values of t_c. In Figure 10(a), occurrence rates for smaller events are relatively constant, while the frequency of occurrence for events with $P > 10$ can differ by an order of magnitude between successive subcatalogs. The changes are significant compared to the data in the inset, showing statistics of five consecutive $2t^*$ subcatalogs from fixed-R cases, where no differences can be observed. Note that the results are robust with respect to the time window chosen (not shown). Models with larger values of t_c (Figs 10b and c) show less pronounced changes at larger potencies, but an increasing change in medium-size seismicity with $10^{-4} < P < 10$. Seismicity rates for large potencies show the largest variability when the dynamics alternate between weakening and strengthening behavior (e.g., for $b = 0.02$, $t_c = 5 \times 10^3$ sec). The changes in seismicity rates are less significant in situations dominated by weakening or strengthening (e.g., for $b = 0.02$, $t_c = 10^4$ sec), yet indicate effects of continuous changes in the frictional properties. The results imply that extrapo-

lations based on past seismicity patterns possibly under or over estimate seismicity rates at later times, depending on the potency range.

5 DISCUSSION

5.1 Comparison to Previous Numerical Studies

We compare our results to previous models that simulate fault zone dynamics. We deliberately parameterize friction evolution in a relatively simple way, following a large body of field and laboratory measurements that are most often parameterized using slip weakening models. Slip weakening is also widely used as a starting parameterization for earthquake simulations, and it is straightforward to construct a case with non-evolving friction. Furthermore, we find that our observations are compatible with models of higher dimensionality and larger internal material degrees of freedom, which use a more detailed but computationally more expensive description of physical mechanisms associated with faulting.

Several studies using multi-cycle simulations explore systematically the effects of frictional and mechanical parameters that control fault zone stability, and discuss the properties of the resulting synthetic seismicity patterns (e. g., Carlson 1991; Rice 1993; Ben-Zion 1996; Langer et al. 1996; Fisher et al. 1997; Dahmen et al. 1998; Shaw & Rice 2000; Lapusta et al. 2000; Weatherley et al. 2002; Heimpel 2003; Zöller et al. 2005a; Mehta et al. 2006; Hillers et al. 2007). Properties such as the energy dissipation and stress interaction distance, dimension, the degree of heterogeneity, and the range of size scales have been used as control parameters. Across a broad range of dimensionality and details of the individual parameterization, structurally disordered faults associated with highly dissipative friction are observed to produce power-law statistics compatible with the Gutenberg-Richter (GR) distribution of seismicity. Relatively homogeneous conditions in tandem with frictional weakening mechanisms lead to slip dominated by characteristic events (CE) with a certain preferred size. These seismicity patterns have been discussed in the context of decreasing geometrical heterogeneity and increasing fault maturity of real faults (Wesnousky 1988, 1994; Stirling et al. 1996). However to date most models have used time independent variations of the control variables, with relatively little attention paid to the feedback mechanisms responsible for the evolution of mechanical and frictional properties. In the earth, such history dependent changes control the evolution of a fault network from an initial, complex state to a later, regularized state. The present study considers these competing feedbacks, focusing on the evolution of the frictional slip weakening rate as a proxy for strengthening and weakening.

Our results are qualitatively compatible with observations made in damage rheology models, that account for plastic deformations and the evolution of the elastic properties of crustal rocks (Lyakhovsky

et al. 1997a,b, 2001; Hamiel et al. 2006). In these studies, the relative efficiency of healing and weakening mechanisms controls the damage distribution and seismic response pattern. In accordance with the damage model (Lyakhovsky et al. 2001), we find that fast (slow) healing, implying weak (strong) memory effects of material weakening and slip localization, tends to produces GR (CE) statistics. In our model, different healing rates are modelled using likely variations of the cutoff time t_c, and small and large values of t_c result in GR and CE frequency-size statistics, respectively.

Studies of granular systems subjected to shear show an evolution of fracture networks (Mora & Place 2002), compatible with the dynamics we observe when weakening dominates in our model. That is, the absence of healing in the granular system causes regions of high shear to remain localized when boundary conditions remain constant. Furthermore, studies on granular materials show that the response of frictional interfaces is highly sensitive to the presence and characteristics of gouge (Place & Mora 1999; Guo & Morgan 2006). While regular stick slip behavior is typically observed for bare surfaces in laboratory experiments and numerical simulations, gouge filled faults shows highly irregular behavior. The jostling and rolling of the constituent particles introduces additional degrees of freedom, analogous to fault zone material and gives rise to additional complexity. This highlights the importance of microscopic interactions, which is implicitly considered in the evolution of the slip weakening rate in the present study.

5.2 Clustering and Mode Switching

We observe for a wide range of healing rates fluctuations in the system dynamics and the corresponding frequency-size statistics that are similar to seismicity clustering observed on real faults. Such a situation emerges for $b = 0.02$ and $t_c = 5 \times 10^3$ sec (Fig. 8), in which the system exhibits behavior reminiscent of clustering or mode switching observed in previous studies (Ben-Zion et al. 1999). For roughly six loading sequences, our system produces excess large events due to an intermittent development of large-R weakening conditions, which are subsequently suppressed by healing and a decrease of R. Figure 10(a) illustrates the associated frequency-size distributions for five consecutive time windows with length $2t^*$. The seismicity rate variations for potencies $\log(P) > 0$ are reminiscent of the temporal clustering of paleoearthquakes on the southern San Andreas fault reported by Biasi et al. (2002, and references therein). Biasi et al. (2002) doubt, however, that segment interaction is a plausible explanation for clustering at this site because of the distance to other seismogenic faults. Our approach provides an alternative explanation, i.e., frictional properties that evolve on time scales comparable to the sequences in these studies may cause an acceleration and subsequent deceleration of activity.

Seismic clustering, both simulated and observed, need not in general develop the clean characteristics

of mode switching observed by Dahmen et al. (1998) and Zöller et al. (2004) (for observational evidence see Ben-Zion 2008). In the Dahmen et al. (1998) and Zöller et al. (2004) studies the statistics switch unambiguously between the GR and CE distributions if values of the fixed, time invariant control parameters such as stress loss (i.e., energy lost due to heat or radiated waves) and heterogeneity are in the vicinity of the GR-CE boundary in the stress loss vs. heterogeneity plane. In these simulations, the duration of a response type is 10 to 100 times a loading cycle, and hence several times larger than the time scales associated with the clustering effect (Biasi et al. 2002). In contrast to the Dahmen and Zöller mode switching but similar to the present results, Lyakhovsky et al. (2001) report mode switching behavior for time scales of a few cycles, with alternating seismicity patterns that are less distinct than those of Dahmen et al. (1998). While the Lyakhovsky et al. (2001) damage rheology produces switching seismicity patterns due to changes in the damage, i.e., fault distribution, our approach implies similar changes in seismic behavior due to evolving frictional properties of existing faults. Note that earthquakes in the damage models are not parameterized by frictional instabilities but correspond to sudden irreversible changes in plastic deformation.

5.3 Nonstationarity and Predictability

The fluctuations responsible for the clustering effects have implications on the predictability of future events due to incomplete or limited knowledge of past seismicity patterns. Our qualitative analysis reaches the conclusion that feedbacks lower the chance of an accurate estimate of future seismicity occurrence.

The nonstationarity of the dynamics with evolving friction—expressed by significant fluctuations in the dynamics—is apparent by comparing the respective measurements (Figs 8 and 9) to the corresponding results of models with time independent friction (Figs 5 and 6). The corresponding fluctuations in the frequency-size distributions (Fig. 10) also highlight the impact of feedbacks on seismicity evolution. The development of a relatively stable dynamic behavior of non-evolving systems, illustrated by small to moderate fluctuations of the E and δE measurements around a stable mean, implies a relatively high predictability of future seismicity based on information of past dynamics. In a system dominated by the occurrence of large and very large events (Fig. 8, $R = 2$), fluctuations occur in the course of the seismic cycle, and patterns may exhibit accelerated moment release of medium-size seismicity while the system approaches the punctuation of a large event (Jaumé & Sykes 1999; Zöller & Hainzl 2002). However, anticipations of seismicity rates for time intervals $>2t^*$ resting on observations of past seismicity are expected to be fairly accurate (Fig. 10a, inset $R = 2$).

In comparison, to assess future behavior of a system with evolving friction on the basis of past pat-

terns, data from much longer times must be evaluated, due to the increased variability in the dynamics and the associated fluctuations in the frequency-size distributions. Thus, extrapolations based on temporally incomplete information regarding past and recent seismicity possibly over or under estimate the occurrence of future seismicity, i.e., statistics on observational time scales may not be reliable predictors of future events.

Biased estimates of magnitude dependent occurrence probabilities can also be based on limited sampling from a fixed statistical distribution (Howell 1985; Kagan 1993). That is, the under estimation of the probability of a large event in Howell (1985) is due to incomplete sampling of a hypothetically complete catalog. However, this mechanism for the variability in event frequency is different from the mechanisms for variability observed in our simulations. Because friction evolution produces statistical distributions that vary with time, the associated variabilities reflect changes in the dynamic regime. In other words, a catalog that contains the complete seismicity of one cycle may still lead to erroneous estimates of seismicity at later times at which the dynamic regime will have changed.

5.4 Fault Zone Evolution and Organizational Principles

The present results show qualitative similarities to models that aim to account for changes of the mechanical properties of crustal material on time scales of fault zone evolution (e.g., Lyakhovsky et al. 2001). To balance b-values, i.e., the slope, of regional Gutenberg-Richter statistics, Wesnousky (1999) suggests a coevolution of fault slip rate and the distribution of faults of a given length. Observations of similar relations, e.g., between the number of faults in a network, their lengths, and the average recurrence intervals of fault-size earthquakes, imply a constant adjustment of fault system properties to evolving tectonics. The evolution from initially heterogeneous to longer aligned simpler faults implies the initiation, growth, and coalescence of faults. Simultaneously certain faults from the initial configuration may heal and cease to be active or exhibit decreased seismicity. The evolutionary path associated with growth and coalescence is similar to the 'weakening' trajectory shown in Figure 9(d). Conversely, the healing and cessation of seismicity, i.e., a decrease of fault-size events, is reminiscent of the 'strengthening' trajectory in Figure 9(d). Furthermore, Wesnousky (1999) discusses that changes in a tectonic regime may lead to the reversal of strain organization, and thus strengthen existing faults and suppress unstable slip.

Strain organization is associated with a tendency to reduce the strain energy (here: E) or configurational entropy more efficiently. This is synonymous with the capability to produce large earthquakes (Main & Burton 1984; Dahmen et al. 1998; Al-Kindy & Main 2003). Weakening dominates the formation, structural evolution, and geometry of mature earthquake faults. This process has been suggested to follow a global minimization principle (Sornette et al. 1994). However, previous approaches do not

consider the effects of competing, potentially reversing restrengthening processes, as we do here.

The process of fault organization, the coevolution of mechanical and frictional properties, and the corresponding seismicity distributions do not necessarily follow a global optimization strategy to exhibit features reminiscent of an optimized or organized system. Rather, an increase in damage and localization associated with the organization and modification of crustal material—wear and breakage, abrasion, material transport—can result just as easily from local and incremental adjustments, as in the development of other internally highly structured systems (Carlson & Doyle 2002). The local, incremental evolution of material properties, e.g., the smoothing of fault surface topography, as well as the passage of seismic waves and hydrothermal conditions occurs across a range of scales. Fault networks containing mature faults represent structured configurations, incrementally organized for a sufficient release of strain energy for the present tectonic situation. The resulting—even intermittently immature—configurations are not random or disorganized, but represent structures with pronounced history dependence which have evolved to their current state through feedbacks coupling material properties and dynamics.

Local incremental algorithms have been shown to lead to characteristics similar to more globally applied optimization schemes (Carlson & Doyle 2000; Robert et al. 2001; Carlson & Doyle 2002; Reynolds et al. 2002; Zhou et al. 2002). Both global and local algorithms can incorporate feedback and efficiency consistent with a minimization principle. Ultimately, the key feature is that the resulting system is more organized than it is random, so that a description based on organization or optimization, rather than the statistics of an ensemble of random configurations, provides a more accurate starting point for modeling. While we expect biological and technological systems to be much closer to optimal than earthquake faults, the basic consequences of system organization through feedbacks, even at a relatively primitive level, are shown here to have a significant influence on the dynamics.

6 CONCLUSIONS

We conducted numerical experiments on an earthquake fault model to investigate the effect of changes in frictional properties of fault zones on seismicity evolution. The model incorporates empirically observed deformation dependent weakening and competing time dependent healing. Together these control the evolution of the frictional slip weakening rate, R. Time independent, fixed values of R result in Gutenberg-Richter and characteristic earthquake frequency-size statistics for small and large R, respectively, reflecting frictional properties associated with early and late stages of wear in deformed materials. More complex system dynamics characterized by larger fluctuations in energy measurements result from slip and time dependent changes of the frictional response. That is, slip dependent

wear and abrasive mechanisms weaken a frictional interface, but hydrothermal processes are responsible for strength recovery during subsequent at-rest periods. Fast acting healing mechanisms, parameterized by relatively small cutoff times, suppress any tendency in a system for the development of persistent weakening dynamics, whereas for less effective healing the weakening mechanisms dominate. For a broad range of intermediate parameter values, measurements of characteristic quantities exhibit significant fluctuations. The time scale of these fluctuations is large compared to fluctuations in the calibration cases with fixed properties. For simulations with fixed, homogeneous friction data covering relatively short time periods give an accurate measure of the bounds of future seismicity, whereas for simulations with evolving friction the extrapolation of temporally limited past seismicity pattern likely over or under estimates properties of future seismicity.

7 ACKNOWLEDGMENTS

We thank A. Martin for the outstanding and timely computational assistance that underpinned much of this work, and M. L. Manning for a critical in-house review that helped to improve the manuscript. G. H. was supported by the Swiss National Science Foundation, contribution number PBEZ2-111586, by the James S. McDonnell Foundation, the David and Lucile Packard Foundation, and the NSF under grant DMR-0606092. This research was supported by the Southern California Earthquake Center. SCEC is funded by NSF Cooperative Agreement EAR-0529922 and USGS Cooperative Agreement 07HQAG0008. The SCEC contribution number for this paper is 1190. The Institute for Crustal Studies contribution number for this paper is 0873. Computations were carried out on the ‘Dragon’ cluster of the Institute for Crustal Studies, University of California, Santa Barbara.

8 APPENDIX

Here we discuss in more detail a variety of physical mechanisms that may influence weakening and strengthening on faults. Our model is sufficiently general to be at least qualitatively consistent with a range of possible mechanisms discussed here.

During the process of strain organization the micro- and macromechanical properties of the involved materials constantly change. These changes affect the stability and dynamics of earthquake faults. The complex multi-scale interactions of the competing weakening and strengthening processes suggest that homogeneous, time independent properties are unlikely to adequately describe the state of fault systems and individual faults. The purpose of this Appendix is to illustrate the breadth of physical processes which may be relevant.

8.0.0.1 Overview Laboratory experiments on rock deformation represent a small scale version of what may happen during fault zone formation. Acoustic emissions reveal that initially formed microcracks coalesce to form slip surfaces, and during this process material properties change significantly in response to irreversible deformations. Despite the wide range of possible and occasionally contradictory responses of crustal material to external forcing—depending on locally variable conditions such as mineral composition, the abundance and phase of fluids, and temperature gradients—fault (system) development can conceptually be characterized by the following sequence: (1) the rheologic weakening of initially intact though probably heterogeneous rock; (2) the localization of deformation accompanied by the regularization of geometric heterogeneities; (3) abrasive mechanisms and wear produce a widening process zone around fault cores, and the formed gouges control the frictional response to forcing; (4) geometric complexities continuously lead to irregularly distributed places of wear and material accumulation.

The development of mature faults, and the adjustment of fault geometries to changes in the tectonic regime expressed by the simultaneous formation of younger structures indicate that properties of regional fault systems change. That is, although mature faults (e.g., the San Andreas fault) accommodate significant portions of relative plate motion, immature faults (e.g., the San Jacinto fault) form in close proximity because the stress field favors strain release in these areas associated with a higher degree of energy dissipation. While fault zone formation and evolution operates on time scales of the order of 10^3 to 10^5 years—at least ten times the cycle duration of large earthquakes—material properties might change over times as small as milliseconds, associated with earthquake rupture propagation.

8.0.0.2 Friction Our model investigates changes in friction behavior due to weakening and strengthening feedbacks. This subsection discusses additional evidence that support the sensitivity of the friction evolution on microscopic conditions.

Rock friction assumes the existence of a sliding surface that may have formed during a breakup process as described above. The leading order static friction coefficient has been found to be independent of rock type (Byerlee 1978). However, the evolution of the frictional resistance during instabilities controls the behavior of earthquake faults, and has been observed to depend on existence, composition and characteristics of gouge, normal stresses, existence of fluids, deformation history, hydrothermal conditions, interevent hold times, and strain and slip rates. Experiments on dry, bare surfaces at room temperature show an inverse proportionality between sliding friction and slip rates (Niemeijer & Spiers 2006, and references therein). Details of friction evolution depend on the roughness of the sliding surfaces, which controls the evolution distance in the rate-and-state framework (Dieterich 1972, 1978), correlating smooth and rough surfaces with effective weakening and strengthening behavior, respec-

tively. A large body of theoretical and numerical work discusses the effects of occasionally subtle changes in the constitutive rate-and-state parameters on system stability (e.g., Rice & Ruina 1983; Rice & Gu 1983; Ruina 1983; Gu et al. 1984; Dieterich 1992; Rubin & Ampuero 2005).

The rate-and-state formulation has been shown to be applicable over a range of quasistatic slip speeds to friction of bare surfaces and the gouge layer, which exhibits a broader response spectrum. Successive wear of contact asperities leads to the formation of gouge (Power et al. 1988; Wang & Scholz 1994; Beeler et al. 1996). According to Lockner & Byerlee (1993) and Beeler et al. (1996), the gouge remains localized exhibiting weakening properties as long as the shear failure strength remains lower than the strength of the surroundings. Beeler et al. (1996) observed in rotary shear experiments of initially bare surfaces an overall velocity weakening, that is interrupted by a period of strengthening behavior. Continued wear results in a widening of the gouge zone (Power et al. 1988; Gu & Wong 1994; Marone 1998a), and its stability sensitively depends on multiple factors. Furthermore, gouge composed of mixtures behaves different from homogeneous materials (Niemeijer & Spiers 2006).

Experimental studies have revealed the critical role of fluids in gouge filled faults (see references in Niemeijer & Spiers 2006), and theoretical studies demonstrated that dilatant gouges under wet conditions can develop properties that suppress unstable slip (e.g., Segall & Rice 1995). A successive organization of material in the fault core possibly leads to hydraulically and thermally isolated structures, that give rise to rapid weakening mechanisms (e.g., Andrews 2006; Rice 2006; Segall & Rice 2006). Although relatively rare, molten material as a result of high slip speeds and thermal isolation (Sibson 1980; Passchier & Trouw 2005; Rempel & Rice 2006; Rice 2006) might further contribute to the formation of spatially heterogeneous fault strength in the aftermath of large slip events.

Common to all laboratory rock experiments is the limitation to relatively small total offsets without bringing the same material in contact over and over again, and the use of relatively straight and planar frictional surfaces or gouge geometries. Furthermore, experiments fail to combine coseismic high slip rates, large displacements and normal stresses associated with crustal dynamic faulting events (Toro et al. 2004). Consequently, most measurements show an initial transient followed by a steady state response (Lee & Rutter 2004). Whereas first order friction effects can be observed analyzing these experiments, important aspects of geometrical heterogeneity can not be addressed.

8.0.0.3 Granular Materials As briefly discussed in Section 5, observations of the highly sensitive and nonlinear dynamics associated with granular materials have important implications for fault zone stability. The notion that fault zone gouge consists of microscopic particles suggests granular materials subject to shear strain may be a proxy of earthquake fault behavior. Furthermore the granular approach to study the evolution of dynamic variables is supported by the occurrence of discontinuities

in the crust, i.e., surfaces within broken material unaffected by healing (Ben-Zion & Sammis 2003). These two observations indicate that the applicability of a discrete, granular approach depends on the scale of the phenomena under investigation.

Ord et al. (2007) discusses the advantage of a discrete particle approach over continuum descriptions to investigate emergent phenomena (Kim 2006) in geo-materials, including fracture evolution and strain localization. In numerical studies of granular systems, simple atomic-bond-like interactions permit the evolution of patterning such as shear bands. Recent work by Langer & Manning (2007) and Langer (2008) has shown, however, that continuum models spontaneously develop shear bands as well. In these continuum models, strain softening emerges naturally from a mean-field description of the microscopic dynamics, in contrast to typical plasticity models where the softening is included only phenomenologically. According to the underlying Shear Transformation Zone (STZ) theory (Falk & Langer 1998, 2000), microscopic configurational rearrangements within the gouge occur much more slowly than macroscopic stress equilibration, suggesting a mechanism for the continued change of a gouge state over long time scales (Manning et al. 2007). Applying the theory within an elastodynamic framework, Daub & Carlson (2008) showed that small differences in shear strain localization influences the nucleation, propagation, and arrest of elastodynamic ruptures and can thus lead to drastically different results for earthquake simulations.

Granular systems subject to shear develop strongly anisotropic time dependent stress fields (Mora & Place 2002; Maloney & Lemaître 2006; Ord et al. 2007), where force chains carry most of the applied load. Furthermore, the relative abundance of different grain shapes within synthetic gouge has strong implications on its stability (Guo & Morgan 2004). Continuous grain comminution affects gouge zone features and thus mechanical properties of fault zones, thereby affecting fault strength and stability (Mora & Place 1999; Guo & Morgan 2006). Spatially variable properties of gouges persist in geometrically simpler fault configurations, resulting in changes of microscopic states even though macroscopically a steady state can be approached (Morgan & Boettcher 1999; Lois et al. 2005). Guo & Morgan (2007) discuss the generally poorly constrained progressive change of granular gouge properties, and observe in their numerical experiment that neither gouge zone thickness nor grain size distribution evolve to a steady state value.

Wear and surface evolution are also reported in shear experiments of non-geo-materials (e.g., Fu et al. 2001a), leading to heterogeneous surface alteration and continued abrasion of nonplanar obstacles. Accompanying molecular dynamics simulations (Fu et al. 2001b) demonstrate the importance of mixing phenomena at all stages of sliding. While Chester & Chester (1998) did not observe mixed material in the fault core during late stages of faulting, competing processes of debris formation and removal

by wear are likely to play a significant role in early and intermediate stages of fault zone evolution.

8.0.0.4 Mechanical Properties of Evolving Fault Zones Since the evolution of friction is the focus of the present study, mechanical properties of the material surrounding faults—represented by the loader spring stiffness k_p (Fig. 1b) in our model—are not discussed. However, changes in the mechanical properties significantly influence the stability of faults, e.g., due to differences in stress buildup and unloading.

The dominant deformation mechanism in relatively young faults is the creation of damaged and broken material through fracturing and comminution. Competing processes like wear, abrasion and the smoothing effects of debris removal tend to decrease structural irregularties. Analysis of exhumed fault sections from midcrustal depths indicate that slip localizes on a relatively narrow zone early in the development, during a stage in which a considerable amount of geometrical complexity still prevails (Chester & Chester 1998; Chester et al. 2004, and references therein). Yield strength and related mechanical rock properties evolve during continued deformation from values of intact rock to the frictional resistance of highly localized shear zones (Cowie & Scholz 1992).

Although structurally simpler, mature faults show roughness at larger scales and wavelengths, and become never perfectly planar and homogeneous. Even very small geometric heterogeneity has strong implications on peak stresses and relaxation at fault irregularities (J. Dieterich, SCEC Earthquake Simulators Workshop, 2008). Continued displacement along nonplanar surfaces results in local stress concentrations responsible for episodic reloading of rocks passing irregularities (Wilson et al. 2003). Wrinkle-like slip pulses associated with rupture along bimaterial interfaces brought into contact as a result of large cumulative offsets (Andrews & Ben-Zion 1997), and the accompanied passage of a rupture tip may also contribute to the accumulation of asymmetric damage patterns. Thus local material properties in the vicinity of a fault are continuously altered (Chester & Chester 1998).

Hong & Menke (2006) estimate the spatial dimension of a wear related zone of the San Jacinto fault and concluded that it extends to depths of the brittle-ductile transition zone, indicating its mechanical importance throughout the seismogenic depth. The analysis of fault zone trapped waves allows the estimate of in-situ large scale wear processes, revealing the existence of a highly fractured zone around the fault core. This low velocity zone, typically a few hundred meters to 1 km wide, persists around large offset faults, consistent with observations from exhumed fault segments. Spatially variable and asymmetric rigidity gradients between intact host rocks and the damaged material (Fialko 2006; Li et al. 2006), and the spatiotemporal variation in strength of strongly deformable low-rigidity compliant zones (Fialko 2004) likely influence the seismic response in an irregular manner. The rheology of

damaged rocks differs in fundamental ways from the reversible deformation associated with Hookean elasticity. Experiments on the response beyond the elastic, linear portion reveal the irreversible change in material properties of highly deformed rock (e.g., Lockner et al. 1991), and are attributed to the density and distribution of microcracks. Continued cyclic loading progressively increases the yield stress at the onset of damage, whereas the material strength decreases with accumulated damage (Hamiel et al. 2006). Permanently deformed rocks dominate crustal properties particularly in tectonically and thus seismically active regions, and the evolving nonlinear response to changing stress states likely influences regional seismicity pattern (e.g., Ben-Zion & Lyakhovsky 2006).

8.0.0.5 The Role of Fluids Fluid assisted processes are implicitly assumed in our model by applying variations in the cutoff time t_c observed by Nakatani & Scholz (2004) conducting fluid saturated friction experiments. The existence and properties of fluid phases in the seismogenic crust, and their effect on fault stability is in general hard to constrain.

Hence, fluids play an important but not well understood role in the earthquake process (Hickman et al. 1995, and references therein). Observational evidence relates fluids to a variety of faulting phenomena, such as fluid driven aftershocks (Nur & Booker 1972; Bosl & Nur 2002; Miller et al. 2004; Piombo et al. 2005), remotely triggered earthquakes (Hill et al. 1993; Husen et al. 2004), generation of aseismic transients, tremors and possibly silent slip events (Segall & Rice 1995; Shibazaki 2005; Liu & Rice 2007). Laboratory experiments investigate the mechanisms responsible for overpressured fluid states (Sleep & Blanpied 1992; Blanpied et al. 1998; Lockner & Byerlee 1994), and highlight the essential role of fluid phases associated with healing and restrengthening (Nakatani & Scholz 2004; Tenthorey & Cox 2006). Byerlee (1990) and Rice (1992) suggest an upward migration of fluids within the damaged fault zone, treating the fault as a sealed conduit, thus explaining the apparent weakness of large faults. Depending on local material properties and rupture histories, fluid pathways can have complex structures (Miller 2006; Sibson 2007), thus leading to heterogeneous and asymmetric patterns of fluid driven processes. The spatially and temporally highly variable distribution of different volatile phases across a fault network, and its multitudinous geochemical, hydrothermal and mechanical implications suggest that an equilibrated state is improbable.

This brief survey, which is far from being exhaustive, suggests that macroscopic properties of fault networks, but also microscopic properties of individual faults, probably do not reach a steady state. While this seems trivial for time scales spanning the dimensions of fault zone formation and development within stable tectonic boundary conditions, mechanisms that change the microstates of frictional interfaces imply that equilibrated conditions are similarly unlikely to be met during shorter time periods.

REFERENCES

Al-Kindy, F. H. & Main, I. G., 2003. Testing self-organized criticality in the crust using entropy: Aregionalized study of the CMT global earthquake catalogue, *J. Geophy. Res.*, **108**(B11).

Andrews, D. J., 2006. Thermal Pressurization Explains Enhanced Long-Period Motion in the Chi-chi Earthquake, *Seism. Res. Let.*, **77**(2), 264.

Andrews, D. J. & Ben-Zion, Y., 1997. Wrinkle-like slip pulse on a fault between different materials, *J. Geophy. Res.*, **102**(B1), 553–571.

Beeler, N. M., Tullis, T. E., Blanpied, M. L., & Weeks, J. D., 1996. Frictional behavior of large displacement experimental faults, *J. Geophy. Res.*, **101**(B4), 8697–8715.

Ben-Zion, Y., 1996. Stress, slip, and earthquakes in models of complex single-fault systems incorporating brittle and creep deformations, *J. Geophy. Res.*, **101**(B3), 5677–5706.

Ben-Zion, Y., 2008. Collective behavior of earthquakes and faults: Continuum-discrete transitions, progressive evolutionary changes and different dynamic regimes, *Rev. Geophys.*, submitted manuscript.

Ben-Zion, Y. & Lyakhovsky, V., 2006. Analysis of aftershocks in a lithospheric model with seismogenic zone governed by damage rheology, *Geophys. J. Int.*, **165**, 197–210.

Ben-Zion, Y. & Sammis, C. G., 2003. Characterization of Fault Zones, *Pure Appl. Geophys.*, **160**, 677–715.

Ben-Zion, Y., Dahmen, K., Lyakhohvsky, V., Ertas, D., & Agnon, A., 1999. Self-driven mode switching of earthquake activity on a fault system, *Earth and Planetary Science Letters*, **172**, 11–21.

Ben-Zion, Y., Eneva, M., & Liu, Y., 2003. Large earthquake cycles and intermittend criticality on heterogeneous faults due to evolving stress and seismicity, *J. Geophy. Res.*, **108**(B6).

Biasi, G. P., II, R. J. W., Fumal, T. E., & Seitz, G. G., 2002. Paleoseismic Event Dating and the Conditional Probability of Large Earthquakes on the Southern San Andreas Fault, California, *Bull. Seism. Soc. Am.*, **92**(7), 2761–2781.

Bizzarri, A. & Cocco, M., 2003. Slip-weakening behavior during the propagation of dynamic ruptures obeying rate- and state-dependent friction laws, *J. Geophy. Res.*, **108**(B8).

Blanpied, M. L., Marone, C. J., Lockner, D. A., Byerlee, J. D., & King, D. P., 1998. Quantitative measure of the variation in fault rheology due to fluid-rock interactions, *J. Geophy. Res.*, **103**(B5), 9691–9712.

Bosl, W. J. & Nur, A., 2002. Aftershocks and pore fluid diffusion following the 1992 Landers earthquake, *J. Geophy. Res.*, **107**(B12).

Burridge, R. & Knopoff, L., 1967. Model and theoretical seismicity, *Bull. Seism. Soc. Am.*, **57**(3), 341–371.

Byerlee, J. D., 1978. Friction of rock, *Pure Appl. Geophys.*, **116**, 615–626.

Byerlee, J. D., 1990. Friction, overpressure and fault normal compression, *Geophys. Res. Lett.*, **17**(12), 2109–2112.

Carlson, J. M., 1991. Time Intervals Between Characteristic Earthquakes and Correlations With Smaller Events: An Analysis Based on a Mechanical Model of a Fault, *J. Geophy. Res.*, **96**(B3), 4255–4267.

Carlson, J. M. & Doyle, J., 2000. Highly Optimized Tolerance: Robustness and Design in Complex Systems, *Phys. Rev. Lett.*, **84**(11), 2529–2532.

Carlson, J. M. & Doyle, J., 2002. Complexity and Robustness, *Proc. Natl. Acad. Sci. USA*, **99**, 2538–2545.

Carlson, J. M. & Langer, J. S., 1989a. Properties of Earthquakes Generated by Fault Dynamics, *Phys. Rev. Lett.*, **62**(22), 2632–2635.

Carlson, J. M. & Langer, J. S., 1989b. Mechanical model of an earthquake fault, *Phys. Rev. A*, **40**(11), 6470–6468.

Carlson, J. M., Langer, J. S., Shaw, B. E., & Tang, C., 1991. Intrinsic properties of a Burridge-Knopoff model of an earthquake fault, *Phys. Rev. A*, **44**(2), 884–897.

Carlson, J. M., Langer, J. S., & Shaw, B. E., 1994. Dynamics of earthquake faults, *Rev. Mod. Phys.*, **66**(2), 657–670, Colloquium Paper.

Chambon, G., Schmittbuhl, J., & Corfdir, A., 2006. Frictional response of a thick gouge sample: 1. Mechanical measurements and microstructures, *J. Geophy. Res.*, **111**.

Chester, F. M. & Chester, J. S., 1998. Ultracataclasite Structure and Friction Processes of the Punchbowl Fault, San Andreas System, California, *Tectonophysics*, **295**, 199–221.

Chester, F. M., Chester, J. S., Kirschner, D. L., Schulz, S. E., & Evans, J. P., 2004. Structure of large-displacement, strike-slip fault zones in the brittle continental crust, in *Rheology and Deformation in the Lithosphere at Continental Margins*, pp. 223–260, eds Karner, G. D., Taylor, B., Driscoll, N. W., & Kohlsted, D. L., Columbia University Press, New York.

Cowie, P. A. & Scholz, C. H., 1992. Physical explanation for the displacement-length relationship of faults using a post-yield fracture mechanics model, *J. Struct. Geol.*, **14**, 1133–1148.

Dahmen, K., Ertas, D., & Ben-Zion, Y., 1998. Gutenberg-Richter and characteristic earthquake behavior in simple mean field models of heterogeneous faults, *Phys. Rev. E*, **58**(2), 1494–1501.

Daub, E. G. & Carlson, J. M., 2008. A constitutive model for fault gouge deformation in dynamic rupture simulations, *J. Geophy. Res.*, submitted.

Dieterich, J. H., 1972. Time-Dependent Friction in Rocks, *J. Geophy. Res.*, **77**(20), 3690–3697.

Dieterich, J. H., 1978. Time-Dependent Friction and the Mechanics of Stick-Slip, *Pure Appl. Geophys.*, **116**, 790–805.

Dieterich, J. H., 1992. Earthquake nucleation on faults with rate- and state-dependent strength, *Tectonophysics*, **211**, 115–134.

Dieterich, J. H. & Kilgore, B. D., 1994. Direct Observation of Frictional Contacts: New Insights for State-dependent Properties, *Pure Appl. Geophys.*, **143**(1/2/3), 283–302.

Falk, M. L. & Langer, J. S., 1998. Dynamics of viscoplastic deformation in amorphous solids, *Phys. Rev. E*, **57**(7192).

Falk, M. L. & Langer, J. S., 2000. From simulation to theory in the physics of deformation and fracture, *M.R.S. Bulletin*, **25**(40).

Fialko, Y., 2004. Probing the mechanical properties of seismically active crust with space geodesy: Study of coseismic deformation due to the 1992 M_w7.3 landers (southern California) earthquake, *J. Geophy. Res.*, **109**.

Fialko, Y., 2006. Interseismic strain accumulation and the earthquake potential on the southern San Andreas fault system, *Nature*, **441**, 968–971.

Fisher, D. S., Dahmen, K., Ramanathan, S., & Ben-Zion, Y., 1997. Statistics of Earthquakes in Simple Models of Heterogeneous Faults, *Phys. Rev. Lett.*, **78**(25), 4885–4888.

Fu, X.-Y., Kasai, T., Falk, M. L., & Rigney, D. A., 2001a. Sliding behavior of metallic glass Part I. Experimental investigations, *WEAR*, **250**, 409–419.

Fu, X.-Y., Kasai, T., Falk, M. L., & Rigney, D. A., 2001b. Sliding behavior of metallic glass Part II. Computer simulations, *WEAR*, **250**, 420–430.

Gu, J.-C., Rice, J. R., Ruina, A. L., & Tse, S. T., 1984. Slip motion and stability of a single degree of freedom elastic system with rate and state dependent friction, *J. Mech. Phys. Solids*, **32**, 167–196.

Gu, Y. & Wong, T.-F., 1994. Development of Shear Localization in Simulated Quartz Gouge: Effect of Cumulative Slip and Gouge Particle Size, *Pure Appl. Geophys.*, **143**(1/2/3), 387–423.

Guo, Y. & Morgan, J. K., 2004. Influence of normal stress and grain shape on granular friction: Results of discrete element simulations, *J. Geophy. Res.*, **109**.

Guo, Y. & Morgan, J. K., 2006. The frictional and micromechanical effects of grain comminution in fault gouge from distinct element simulations, *J. Geophy. Res.*, **111**.

Guo, Y. & Morgan, J. K., 2007. Fault gouge evolution and its dependence on normal stress and rock strength—Results of discrete element simulations: Gouge zone properties, *J. Geophy. Res.*, **111**.

Hamiel, Y., Katz, O., Lyakhovsky, V., Reches, Z., & Fialko, Y., 2006. Stable and unstable damage evolution in rocks with implications to fracturing of granite, *Geophys. J. Int.*, **167**, 1005–1016.

Heimpel, M. H., 2003. Characteristic scales of earthquake rupture from numerical models, *Nonlinear Processes in Geophysics*, **10**(6), 573–584.

Hickman, N. M. B. S. H. & Wong, T.-F., 2001. Earthquake stress drop and laboratory-inferred interseismic strength recovery, *J. Geophy. Res.*, **106**, 30,701–30,713.

Hickman, S., Sibson, R., & Bruhn, R., 1995. Introduction to special section: Mechanical involvement of fluids in faulting, *J. Geophy. Res.*, **100**(B7), 12,831–12,840.

Hill, D. P., Reasenberg, P. A., & others, ., 1993. Seismicity Remotely Triggered by the Magnitude 7.3 Landers, California, Earthquake, *Science*, **260**(5114), 1617–1623.

Hillers, G., Mai, P. M., Ben-Zion, Y., & Ampuero, J. P., 2007. Statistical properties of seismicity of fault zones at different evolutionary stages, *Geophys. J. Int.*, (169), 515–533.

Hiramatsu, Y., Honma, H., Saiga, A., Furumoto, M., & Ooida, T., 2005. Seismological evidence on characteristic time of crack healing in the shallow crust, *Geophys. Res. Lett.*, **32**.

Hong, T.-K. & Menke, W., 2006. Tomographic investigation of the wear along the San Jacinto fault, southern California, *Phys. Earth Planet. Inter.*, **155**, 236–248.

Howell, B. F., 1985. On the effect of too small a data base on earthquake frequency diagrams, *Bull. Seism. Soc. Am.*, **75**(4), 1205–1207.

Husen, S., Taylor, R., Smith, R. B., & Healser, H., 2004. Changes in geyser eruption behavior and remotely

triggered seismicity in Yellowstone National Park produced by the 2002 M 7.9 Denali fault earthquake, Alaska, *Geology*, **32**(6), 537–540.

Jaumé, S. C. & Sykes, L. R., 1999. Evolving Towards a Critical Point: A Review of Accelerating Seismic Moment/Energy Release Prior to Large and Great Earthquakes, *Pure Appl. Geophys.*, **155**, 279–306.

Kagan, Y. Y., 1993. Statistics of Characteristic Earthquakes, *Bull. Seism. Soc. Am.*, **83**(1), 7–24.

Kim, J., 2006. Emergence: Core ideas and issues, *Synthese*, **151**, 547–559.

Langer, J. S., 2008. Shear-transformation-zone theory of plastic deformation near the glass transition, *Phys. Rev. E*, **77**, 021502.

Langer, J. S. & Manning, M. L., 2007. Steady-state, effective-temperature dynamics in a glassy material, *Phys. Rev. E*, **76**, 056107.

Langer, J. S., Carlson, J. M., Myers, C. R., & Shaw, B. E., 1996. Slip complexity in dynamic models of earthquake faults, *Proc. Natl. Acad. Sci. USA*, **93**, 3825–3829, Colloquium Paper.

Lapusta, N., Rice, J. R., Ben-Zion, Y., & Zheng, G., 2000. Elastodynamic analysis for slow tectonic loading with spontaneous rupture episodes on faults with rate- and state-dependent friction, *J. Geophy. Res.*, **105**(B10), 23,765–23,789.

Lee, A. G. G. & Rutter, E. H., 2004. Experimental rock-on-rock frictional wear: Application to subglacial abrasion, *J. Geophy. Res.*, **109**.

Li, Y.-G., Chen, P., Cochran, E. S., Vidale, J. E., & Burdette, T., 2006. Seismic Evidence for Rock Damage and Healing on the San Andreas Fault Associated with the 2004 **M**6.0 Parkfield Earthquake, *Bull. Seism. Soc. Am.*, **96**(4B), S349–S363.

Liu, Y. & Rice, J. R., 2007. Spontaneous and triggered aseismic deformation transients in a subduction fault model, *J. Geophy. Res.*, **112**.

Lockner, D. A. & Byerlee, J. D., 1993. How geometrical constraints contribute to the weakness of mature faults, *Nature*, **363**, 250–252.

Lockner, D. A. & Byerlee, J. D., 1994. Dilatancy in hydraulically isolated faults and the suppression of instability, *Geophys. Res. Lett.*, **21**(22), 2353–2356.

Lockner, D. A., Byerlee, J. D., Kuksenko, V., Ponomarev, A., & Sidorin, A., 1991. Quasi-static fault growth and shear fracture energy in granite, *Nature*, **350**, 39–42.

Lois, G., Lemaître, A., & Carlson, J. M., 2005. Numerical tests of constitutive laws for dense granular flows, *Phys. Rev. E*, **72**(5), 051303.

Lyakhovsky, V., Ben-Zion, Y., & Agnon, A., 1997a. Distributed damage, faulting, and friction, *J. Geophy. Res.*, **102**(B12), 27,635–27,649.

Lyakhovsky, V., Reches, Z., Weinberger, R., & Scott, T. E., 1997b. Non-linear elastic behavior of damaged rocks, *Geophys. J. Int.*, **130**, 157–166.

Lyakhovsky, V., Ben-Zion, Y., & Agnon, A., 2001. Earthquake cycle, fault zones, and seismicity patterns in a rheologically layered lithosphere, *J. Geophy. Res.*, **106**(B3), 4103–4120.

Main, I. G. & Burton, P. W., 1984. Information theory and the earthquake frequency-magnitude distribution,

Bull. Seism. Soc. Am., **74**(4), 1409–1426.

Maloney, C. E. & Lemaître, A., 2006. Amorphous systems in athermal, quasistatic shear, *Phys. Rev. E*, **74**(016118).

Manning, M. L., Langer, J. S., & Carlson, J. M., 2007. Strain localization in a shear transformation zone model for amorphous solids, *Phys. Rev. E*, **76**, 056106.

Marone, C., 1998a. Laboratory-derived friction laws and their application to seismic faulting, *Annu. Rev. Earth Planet. Sci.*, **26**, 643–696.

Marone, C., 1998b. Laboratory-derived friction laws and their application to seismic faulting, *Nature*, **391**, 69–72.

Marone, C. & Kilgore, B., 1993. Scaling of the critical slip distance for seismic faulting with shear strain in fault zones, *Nature*, **362**, 618–621.

Marone, C., Vidale, J. E., & Ellsworth, W. L., 1995. Fault healing inferred from time dependent variations in source properties of repeating earthquakes, *Geophys. Res. Lett.*, **22**(22), 3095–3098.

Mehta, A. P., Dahmen, K. A., & Ben-Zion, Y., 2006. Universal mean moment rate profiles of earthquake ruptures, *Phys. Rev. E*, **73**.

Miller, S. A., 2006. Fluid-Controlled Aftershock Patterns from Different Tectonic Regimes, *Eos Trans. AGU*, **87**(52), Fall. Meet. Suppl., Abstract T12A-08.

Miller, S. A., Collettini, C., Chiaraluce, L., Cocco, M., Barchi, M., & Kaus, J. P., 2004. Aftershocks driven by a high-pressure CO_2 source at depth, *Nature*, **427**, 724–727.

Mora, P. & Place, D., 1999. The weakness of earthquake faults, *Geophys. Res. Lett.*, **26**(1), 123–126.

Mora, P. & Place, D., 2002. Stress Correlation Function Evolution in Lattice Solid Elasto-dynamic Models of Shear and Fracture Zones and Earthquake Prediction, *Pure Appl. Geophys.*, **159**, 2413–1427.

Morgan, J. K. & Boettcher, M. S., 1999. Numerical simulations of granular shear zones using the distinct element method 1. Shear zone kinematics and the micromechanics of localization, *J. Geophy. Res.*, **104**(B2), 2703–2719.

Nakatani, M. & Scholz, C. H., 2004. Frictional healing of quartz gouge under hydrothermal conditions: 1. Experimental evidence for solution transfer healing mechanism, *J. Geophy. Res.*, **109**(B07201).

Nakatani, M. & Scholz, C. H., 2006. Intrinsic and apparent short-time limits for fault healing: Theory, observations, and implications for velocity-dependent friction, *J. Geophy. Res.*, **111**(B12208).

Niemeijer, A. R. & Spiers, C. J., 2006. Velocity dependence of strength and healing behaviour in simulated phyllosilicate-bearing fault gouge, *Tectonophysics*, **427**, 231–253.

Nur, A. & Booker, J. R., 1972. Aftershocks Caused by Pore Fluid Flow?, *Science*, **175**, 885–887.

Ohnaka, M., 2003. A constitutive scaling law and a unified comprehension for frictional slip failure, shear fracture of intact rock, and earthquake rupture, *J. Geophy. Res.*, **108**(B2).

Ord, A., Hobbs, B., & Regenauer-Lieb, K., 2007. Shear band emergence in granular materials—A numerical study, *Int. J. for Numerical and Analytical Methods in Geomechanics*, **31**, 373–393.

eds Passchier, C. W. & Trouw, R. A. J., 2005. *Microtectonics*, Springer, Berlin, 2nd edn.

Perfettini, H., Campillo, M., & Ionescu, I., 2003. On the scaling of the slip weakening rate of heterogeneous faults, *J. Geophy. Res.*, **108**(B9).

Piombo, A., Martinelli, G., & Dragoni, M., 2005. Post-seismic fluid flow and Coulomb stress changes in a poroelastic medium, *Geophys. J. Int.*, **162**, 507–515.

Place, D. & Mora, P., 1999. The lattice solid model to simulate the physics of rocks and earthquakes: Incorporation of friction, *J. Comp. Phys.*, **150**, 332–372.

Power, W. L., Tullis, T. E., & Weeks, J. D., 1988. Roughness and wear during brittle failure, *J. Geophy. Res.*, **98**, 15268–15278.

eds Press, W. H., Teukolsky, S. A., Vetterling, W. T., & Flannery, B. P., 1992. *Numerical Recipes in FORTRAN: The Art of Scientific Computing*, Cambridge Univ. Press, Cambridge, 2nd edn.

Rempel, A. W. & Rice, J. R., 2006. Thermal pressurization and onset of melting in fault zones, *J. Geophy. Res.*, **111**(B09314).

Reynolds, D., Carlson, J. M., & Doyle, J., 2002. Design degrees of freedom and mechanisms for complexity, *Phys. Rev. E*, **66**(1), 016108.

Rice, J. R., 1992. Fault Stress States, Pore Pressure Distributions, and the Weakness of the San Andreas Fault, in *Fault Mechanics and Transport Properties in Rocks*, pp. 475–503, eds Evans, B. & Wong, T.-F., Academic Press, San Diego, Calif.

Rice, J. R., 1993. Spatio-temporal Complexity of Slip on a Fault, *J. Geophy. Res.*, **98**(B6), 9885–9907.

Rice, J. R., 2006. Heating and weakening of faults during earthquake slip, *J. Geophy. Res.*, **111**(B05311).

Rice, J. R. & Gu, J.-C., 1983. Earthquake Aftereffects and Triggered Seismic Phenomena, *Pure Appl. Geophys.*, **121**(2), 187–219.

Rice, J. R. & Ruina, A. L., 1983. Stability of steady frictional slipping, *J. Appl. Mech.*, **50**, 343–349.

Richardson, E. & Marone, C., 1999. Effect of normal stress vibrations on frictional healing, *J. Geophy. Res.*, **104**(B12), 28,859–28,878.

Robert, C., Carlson, J. M., & Doyle, J., 2001. Highly optimized tolerance in epidemic models incorporating local optimization and regrowth, *Phys. Rev. E*, **63**(5), 056122.

Rubin, A. M. & Ampuero, J.-P., 2005. Earthquake nucleation on (aging) rate and state faults, *J. Geophy. Res.*, **110**(B11312).

Ruina, A., 1983. Slip Instability and State Variable Friction Laws, *J. Geophy. Res.*, **88**(B12), 10,359–10,370.

Sammis, C. G. & Sornette, D., 2002. Positive feedback, memory, and the predictability of earthquakes, *Proc. Natl. Acad. Sci. USA*, **99**, 2501–2508, Colloquium Paper.

ed. Scholz, C. H., 1990. *The mechanics of earthquakes and faulting*, Cambridge University Press, Cambridge, 1st edn.

Segall, P. & Rice, J. R., 1995. Dilatancy, compaction, and slip instability of a fluid-infiltrated fault, *J. Geophy. Res.*, **100**(B11), 22,155–22,171.

Segall, P. & Rice, J. R., 2006. Does shear heating of pore fluid contribute to earthquake nucleation?, *J. Geophy. Res.*, **111**(B09316).

Shaw, B. E. & Rice, J. R., 2000. Existence of continuum complexity in the elastodynamics of repeated fault ruptures, *J. Geophy. Res.*, **105**(B10), 23,791–23,810.

Shibazaki, B., 2005. Nucleation process with dilatant hardening on a fluid-infiltrated strike-slip fault model using a rate- and state-dependent friction law, *J. Geophy. Res.*, **110**.

Sibson, R. H., 1980. Transient discontinuities in ductile shear zones, *J. Struct. Geol.*, **2**(1/2), 165–171.

Sibson, R. H., 2007. An episode of fault-valve behavior during compressional inversion?—The 2004 M_J6.8 Mid-Niigata Prefecture, Japan, earthquake sequence, *Earth and Planetary Science Letters*, **257**, 188–199.

Sleep, N. H. & Blanpied, M. L., 1992. Creep, compaction and the weak rheology of major faults, *Nature*, **359**, 687–692.

Sornette, D., Miltenberger, P., & Vanneste, C., 1994. Statistical Physics of Fault Patterns Self-organized by Repeated Earthquakes, *Pure Appl. Geophys.*, **142**, 491–527.

Stirling, M. W., Wesnousky, S. G., & Shimazaki, K., 1996. Fault Trace Complexity, Cumulative Slip, and the Shape of the Magnitude-frequency Distribution for Strike-slip Faults: A Global Survey, *Geophys. J. Int.*, **124**, 833–868.

Tenthorey, E. & Cox, S. F., 2006. Cohesive strengthening of fault zones during the interseismic period: An experimental study, *J. Geophy. Res.*, **111**.

Toro, G. D., Goldsby, D. L., & Tullis, T. E., 2004. Friction falls towards zero in quartz rock as slip velocity approaches seismic rates, *Nature*, **427**, 436–439.

Vidale, J. E., Ellsworth, W. L., Cole, A., & Marone, C., 1994. Variations in rupture process with recurrence interval in a repeated small earthquake, *Nature*, **368**, 624–262.

Wang, W. & Scholz, C. H., 1994. Wear processes during frictional sliding of rock: A theoretical and experimental study, *J. Geophy. Res.*, **99**(B4), 6789–6799.

Weatherley, D., Mora, P., & Xia, M. F., 2002. Long-range Automaton Models of Earthquakes: Power-law Accelerations, Correlation Evolution, and Mode-switching, *Pure Appl. Geophys.*, **159**, 2469–2490.

Wesnousky, S. G., 1988. Seismological and structural evolution of strike-slip faults, *Nature*, **335**, 340–343.

Wesnousky, S. G., 1994. The Gutenberg-Richter or Characteristic Earthquake Distribution, Which Is It?, *Bull. Seism. Soc. Am.*, **84**(6), 1940–1959.

Wesnousky, S. G., 1999. Crustal Deformation Processes and the Stability of the Gutenberg-Richter Relationship, *Bull. Seism. Soc. Am.*, **89**(4), 1131–1137.

Wilson, J. E., Chester, J. S., & Chester, F. M., 2003. Microfracture analysis of fault growth and wear processes, Punchbowl Fault, San Andreas system, California, *J. Struct. Geol.*, **25**, 1855–1873.

Xia, J., Gould, H., Klein, W., & Rundle, J. B., 2005. Simulations of the Burridge-Knopoff Model of Earthquakes with Variable Range Stress Transfer, *Phys. Rev. Lett.*, **95**(24).

Yasuhara, H., Marone, C., & Ellsworth, D., 2005. Fault zone restrengthening and frictional healing: The role of pressure solution, *J. Geophy. Res.*, **110**.

Zhou, T., Carlson, J. M., & Doyle, J., 2002. Mutation, specialization, and hypersensitivity in highly optimized tolerance, *Proc. Natl. Acad. Sci. USA*, **99**(4), 2049–2054.

Zöller, G. & Hainzl, S., 2002. A systematic spatiotemporal test of the critical point hypothesis for large earthquakes, *Geophys. Res. Lett.*, **29**.

Zöller, G., Hohlschneider, M., & Ben-Zion, Y., 2004. Quasi-static and Quasi-dynamic Modeling of Earthquake Failure at Intermediate Scales, *Pure Appl. Geophys.*, **161**, 2103–2118.

Zöller, G., Hainzl, S., Hohlschneider, M., & Ben-Zion, Y., 2005a. Aftershocks resulting from creeping sections in a heterogeneous fault, *Geophys. Res. Lett.*, **32**.

Zöller, G., Hohlschneider, M., & Ben-Zion, Y., 2005b. The role of heterogeneities as a tuning parameter of earthquake dynamics, *Pure Appl. Geophys.*, **162**, 1027–1049.

	Observation	Scale	Context / Conditions	Model Implementation
Weakening	(i) Diplacement at which d_c reaches a lower, constant value	10^{-3} m	Laboratory experiments of friction with gouge	Upscale observations from microscopic scales (i) to (iii) to account for macroscopic conditions; Use upscaled stability transition distance $d_t = D_0$ (~ 10 m)
	(ii) Displacement at which accumulation of gouge changes	10^{-2} m	Numerical experiments of particle ensembles	
	(iii) Displacement at which wear rate changes	10^{-1} m	Laboratory experiments of frictional surfaces	
	(iv) Displacement associated with regularization of fault traces	10^{5} m	Measurement of fault zone heterogeneity	
Healing	Healing rate b	10^{-2}	Measurements in friction experiments	Use $b = 0.01$ and $b = 0.02$.
	Cutoff time t_c	$1 - 10^5$ sec	Measurements in friction experiments with variable hydrothermal conditions	Use $5 \leq t_c \leq 2 \times 10^5$ sec

Table 1. Summary of the length and time scales associated with weakening and healing mechanisms discussed in the text. The relevant references are given in Section 4.2.1. The displacements in (i) to (iv) refer to a distance d_t associated with the transition from strengthening to weakening behavior. This transition corresponds to the localization of deformation in gouge layers in (i) to (iii), and to the reduction of fault trace heterogeneity in (iv) that allows large ruptures to propagate.

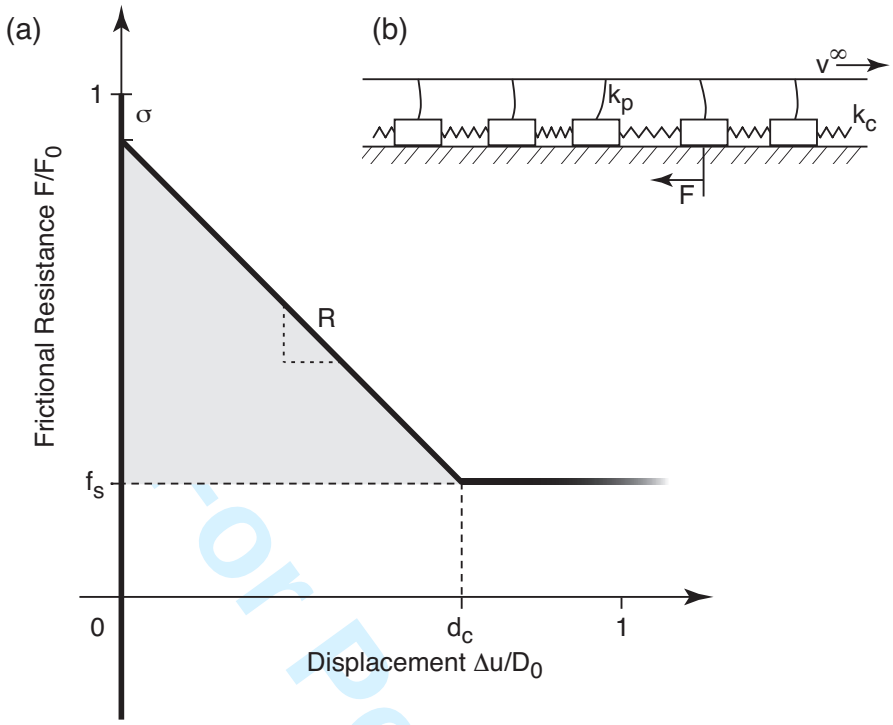

Figure 1. (a) Sketch of the slip weakening friction given in Equation 7; and (b) the mechanical model described by Equation 3. The velocity of the loader plate is v^{∞}, and the loader spring and block connecting spring constants are k_p and k_c, respectively. The motion of a block is controlled by the friction in (a). If the force on a block, K, reaches the peak strength $F = F_0$, F drops to $F = F_0(1 - \sigma)$. During unstable slip $\Delta u > 0$, the frictional strength decreases with rate R to the sliding level, $F = F_0 f_s$, at $\Delta u = d_c$. The grey shaded area is proportional to the fracture energy G. The smaller G, the weaker a fault behaves, and instabilities tend to grow more easily.

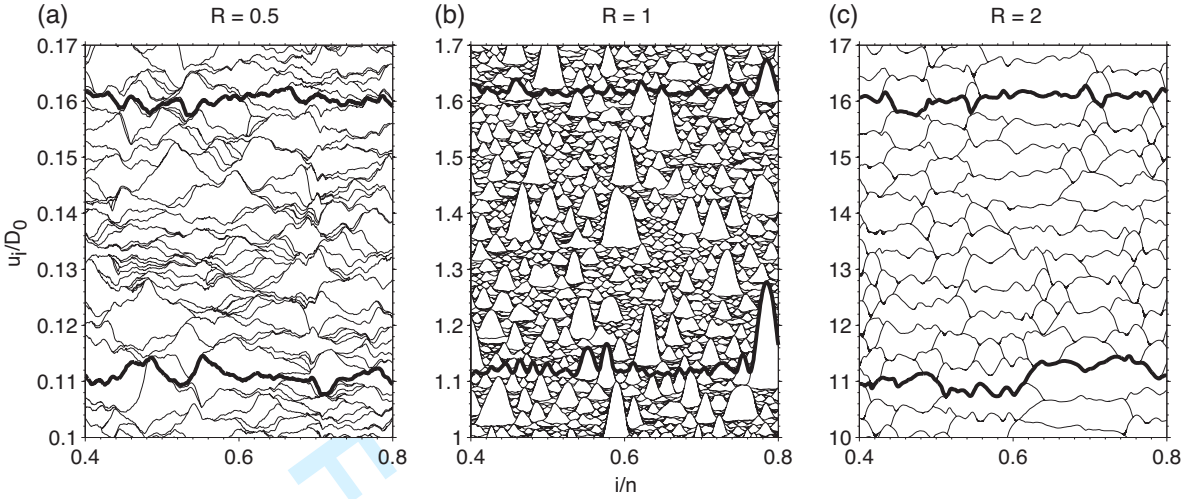

Figure 2. Spatiotemporal slip patterns for systems with $f_s = 0.5$ and variable values of the slip weakening rate, R. The horizontal lines represent the position of blocks after each slip event. In (a) to (c) thick solid lines are drawn every $0.05t^*$, $0.5t^*$, and $5t^*$, respectively. The abscissa denotes the position of individual blocks, i, as a fraction of the system size, n. Note the magnitude differences on the vertical axis, necessary to visually capture the system characteristics. (a) A small weakening rate, associated with a large fracture energy, prohibits the accumulation of slip during instabilities and reflects overall strengthening. (b) $R = 1$ leads to increased slip during unstable episodes and consequently the slip pattern consists of larger events. (c) Large, delocalized events dominate the system response due to a relatively large weakening rate.

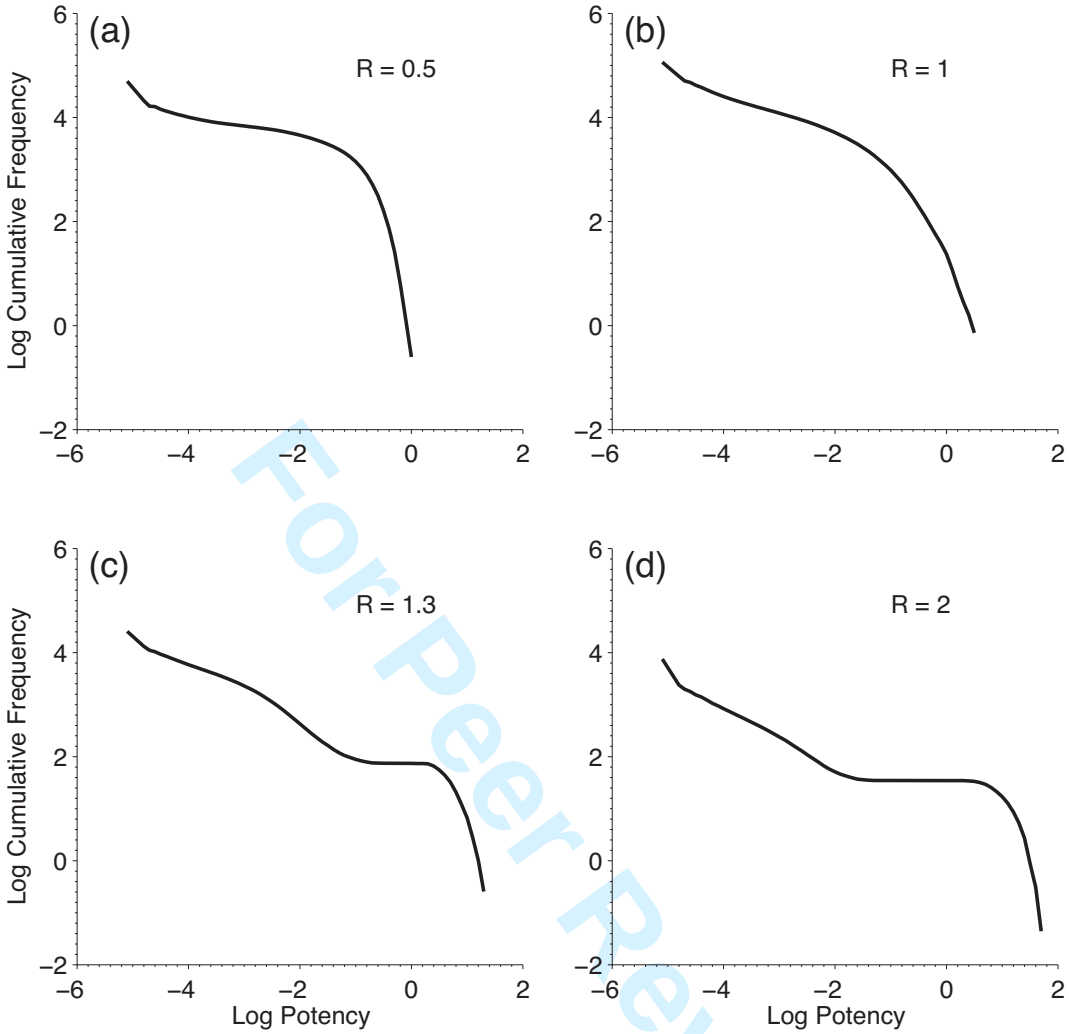

Figure 3. Frequency-size statistics of synthetic earthquakes produced by increasing weakening rates, R, and a constant frictional sliding level, f_s (cf. Fig. 2). The potency is defined in Equation 6. The frequency of occurrence is scaled to the rate per loading cycle, t^*. Relatively small R values result in an approximate power-law scaling for small and moderate events, and an exponential taper towards larger events (a and b). Larger weakening rates produce distributions that are dominated by large sizes, with an increasing gap in medium size seismicity for increasing R. The transition between these commonly referred to Gutenberg-Richter (GR) and characteristic earthquake (CE) statistics occurs around $R = 1$. The tendency to produce delocalized events associated with larger rates leads to successively larger maximum event sizes, a lower productivity (number of events per unit time), and an increase in the slope of the approximately power-law scaling small event population.

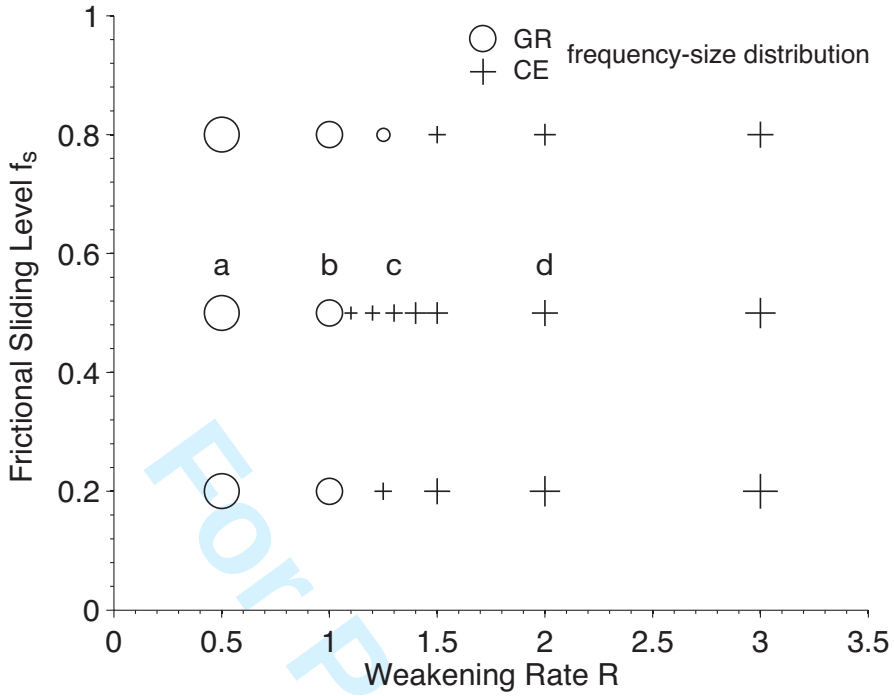

Figure 4. Overview of the observed response types as a function of the fixed dynamic variables sliding level and weakening rate, f_s and R, respectively. Circles and plus signs represent GR and CE statistics, respectively, and the symbol size represents the qualitative 'match' to these labels. Large circles denote approximate power-law scaling for small and moderate events and an exponential taper for larger events (Fig. 3a). Statistics associated with smaller circles show a steeper slope and a less pronounced exponential tail. Large plus signs stand for distributions that are dominated by very large event sizes, with a significant gap in medium size seismicity. For smaller plus signs the gap and the maximum event size becomes smaller (Fig. 3d). Labels 'a' to 'd' correspond to Figures 3(a) to (d). The strongest sensitivity in the system behavior is associated with changes in R. For $R < 1$, the maximum $f_s = 0.8$ considered here is not reached during unstable slip of an individual block, which explains the constant circle size for $R \leq 1$.

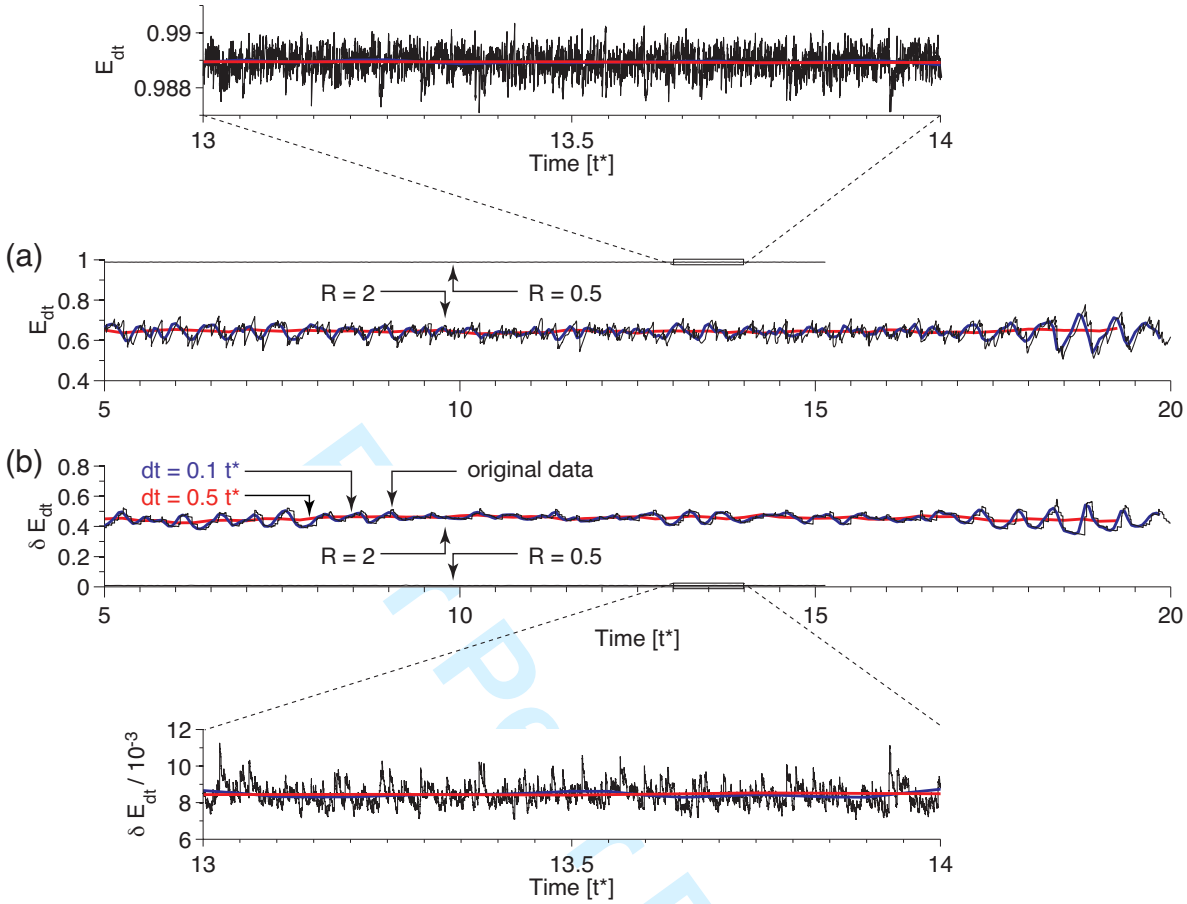

Figure 5. Temporal evolution of the (scaled) average energy (after every single event) and energy fluctuations, (a) E_{dt} (Eq. 4) and (b) δE_{dt} (Eq. 5), respectively, for systems with $R = 0.5$ and $R = 2$ in Figures 3(a) and (d) and 4(a) and (c). The black lines show data after each event, while the blue and red lines show values averaged over time windows of length $dt = 0.1t^*$ and $dt = 0.5t^*$ and overlap $dt/2$, respectively. In the small-R case the energy level close to unity implies a relatively small release of stored energy (Fig. 2a), and tiny fluctuations indicate a high degree of synchronization. Note that the functions for $R = 0.5$ in (a) and (b) appear as a straight line. The large-R system exhibits larger E_{dt} amplitudes around a lower mean level, associated with the efficient energy release of large events. Consequently, the resulting block configurations are less synchronized and exhibit higher energy fluctuations δE_{dt}.

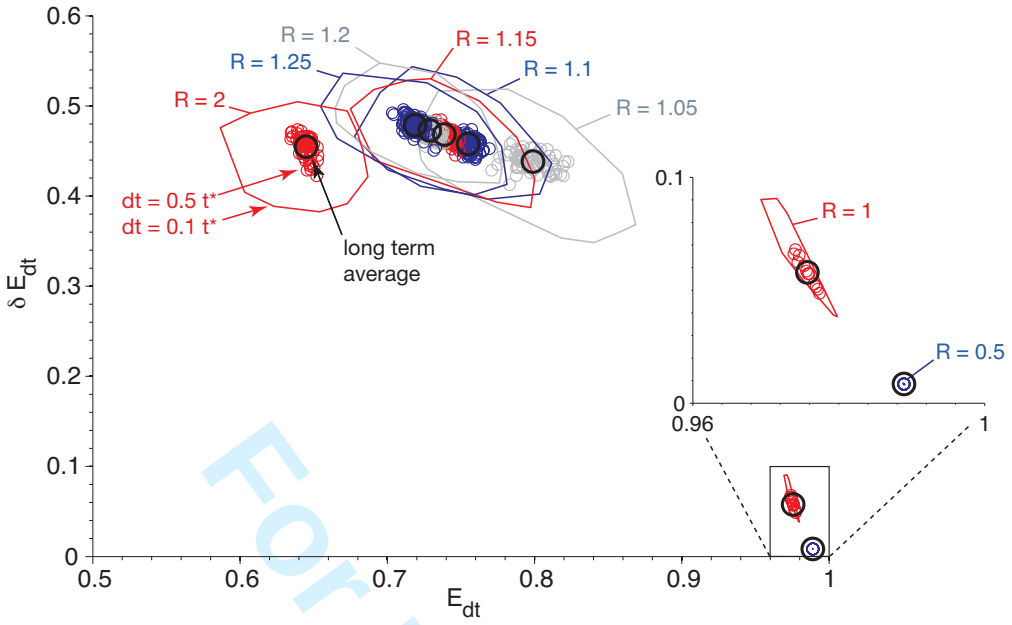

Figure 6. Representation of system dynamics in the E_{dt} (mean energy) vs. δE_{dt} (energy fluctuations) plane. Data are averaged over two different time windows of length $dt = 0.1t^*$ and $dt = 0.5t^*$. The colored circles correspond to results for $dt = 0.5t^*$, using different values of R. The polygons indicate the envelope of data points for $dt = 0.1t^*$. Similar to Figure 5, a successive increase of dt reduces the scatter and tends to confine the data around the long term temporal average (black circles).

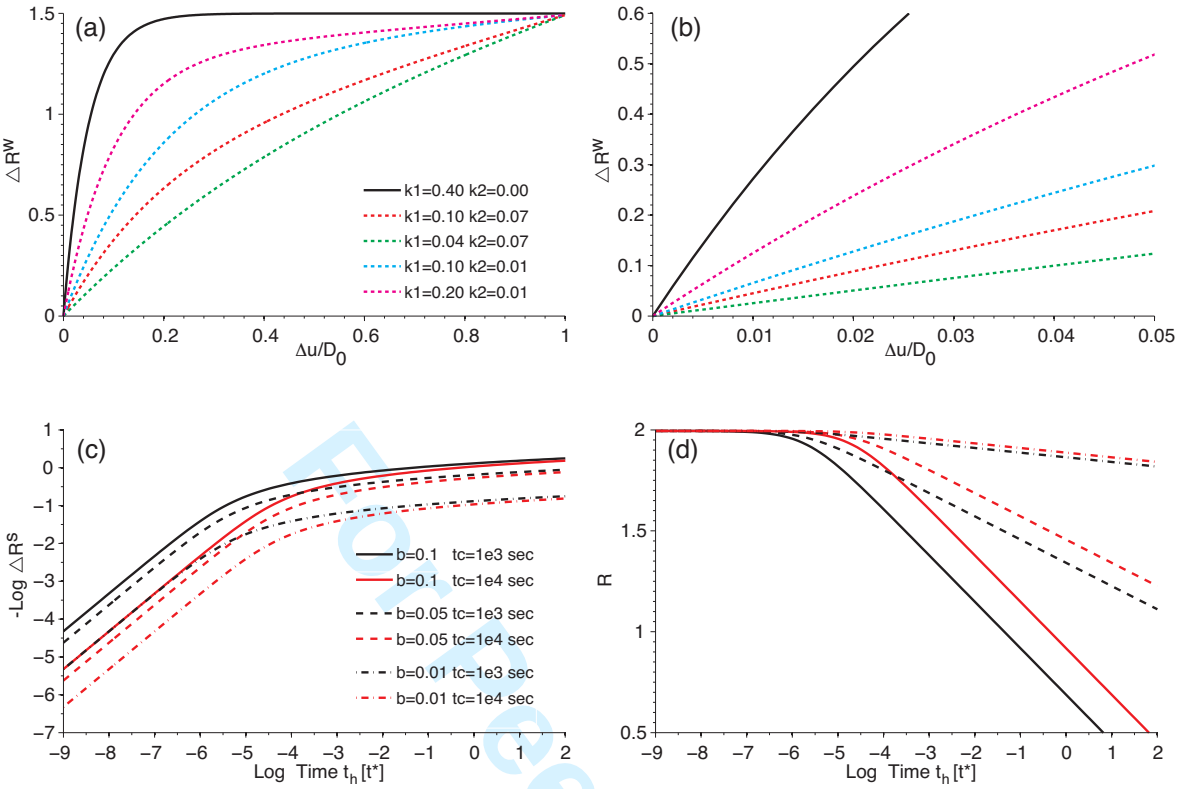

Figure 7. Graphical representation of the evolution functions representing weakening (Eq. 1) and healing (Eq. 2), obtained from interpretations of laboratory experiments by Wang & Scholz (1994) and Nakatani & Scholz (2004, 2006), respectively. (a) Slip induced weakening of ΔR^w, depending on k_1 and k_2. The scaling parameters of Equation 1, γ_0 and A, have been chosen appropriately to change R from 0.5 to 2 (cf. Fig. 4) over the sliding distance $\Delta u = D_0$, i.e., $\Delta R^w_{\max} = 1.5$. (b) Magnification of (a) for small offsets. (c) Changes in R as a function of hold time, t_h, for different combinations of the healing parameter b, and the cutoff time, t_c. (d) Illustration of Equation 9, with $R^{1+} = 2$ and ΔR^s as in (c).

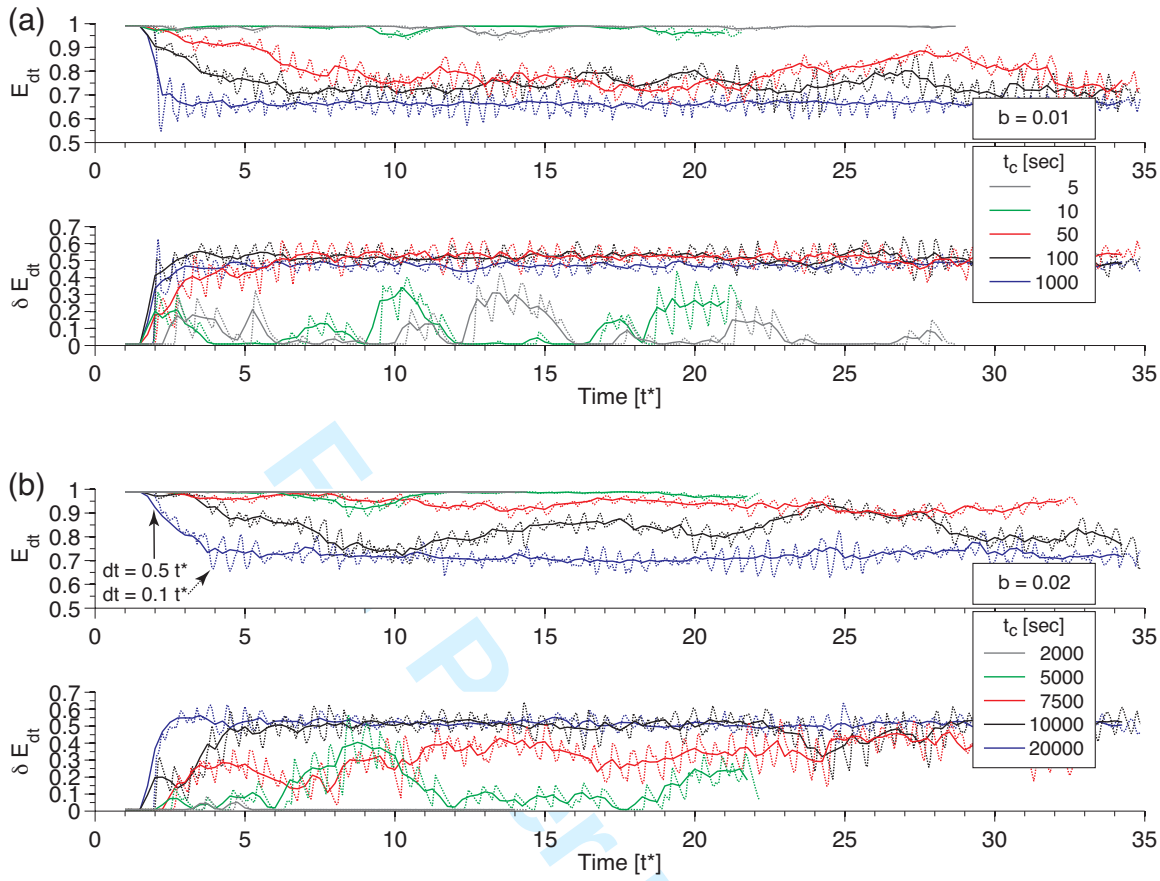

Figure 8. Temporally averaged values of E_{dt} and δE_{dt}, with $dt = 0.1t^*$ (dashed) and $dt = 0.5t^*$ (solid), from simulations with variable values of the healing parameter b and t_c. The weakening parameters are held constant, using the values that correspond to the black line in Figures 7(a) and (b).

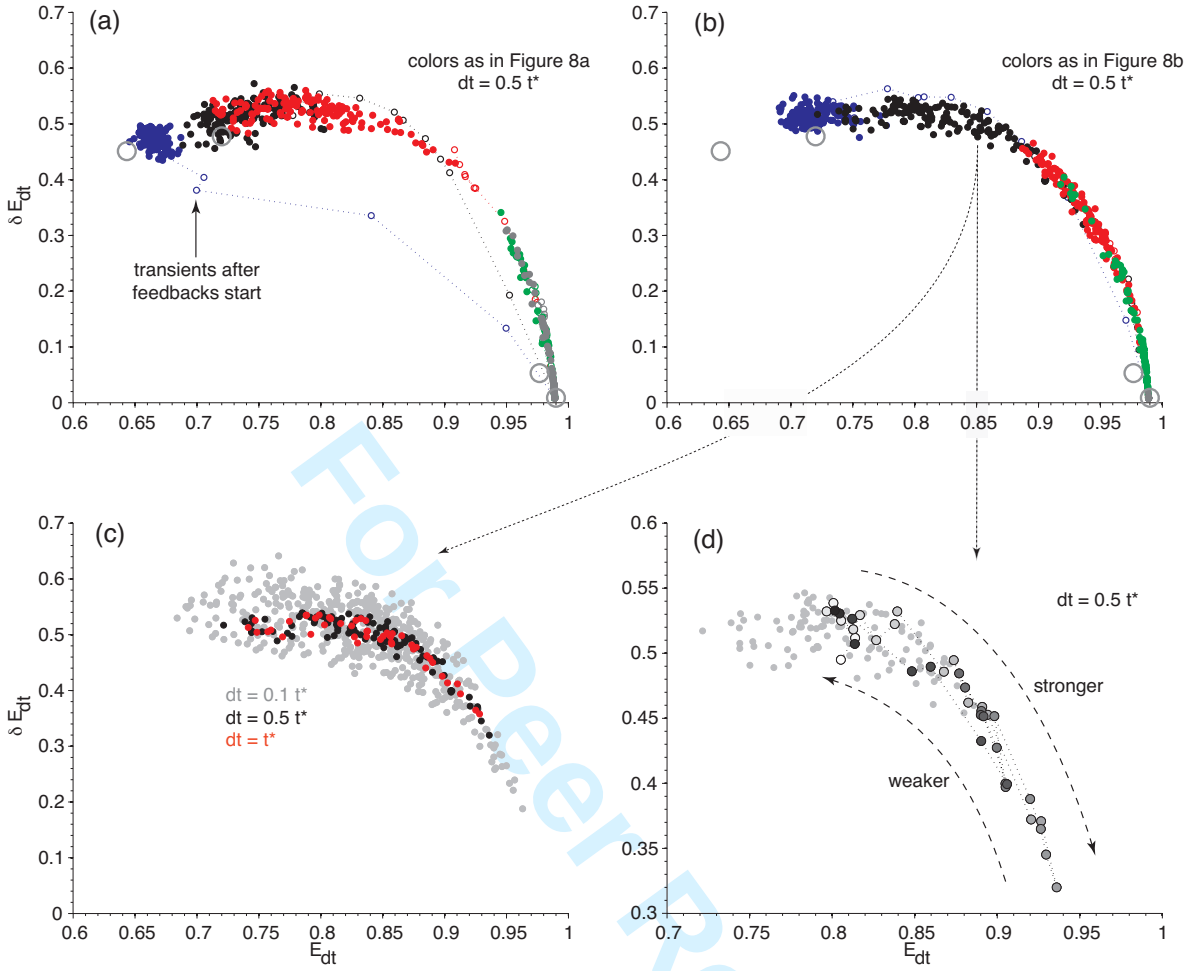

Figure 9. Representation of the data shown in Figure 8 in the E_{dt} vs. δE_{dt} plane. (a) & (b) Small open circles denote the transient effects after the feedbacks started to operate. The four grey circles correspond to the stable mean values of the systems with fixed properties discussed in Figure 6. Here, $dt = 0.5\,t^*$. (c) & (d) Data from (b), $b = 0.02$, $t_c = 10^4$ sec. (c) Data averaged over three different time windows, $dt = 0.1t^*$, $dt = 0.5t^*$, and $dt = t^*$. (d) Light grey dots show data for all times, while progressively darker circles illustrate the temporal evolution for $20t^* < t < 30t^*$ (Fig. 8b, black). A $5\,t^*$-period of motion towards more strengthening behavior is subsequently reversed.

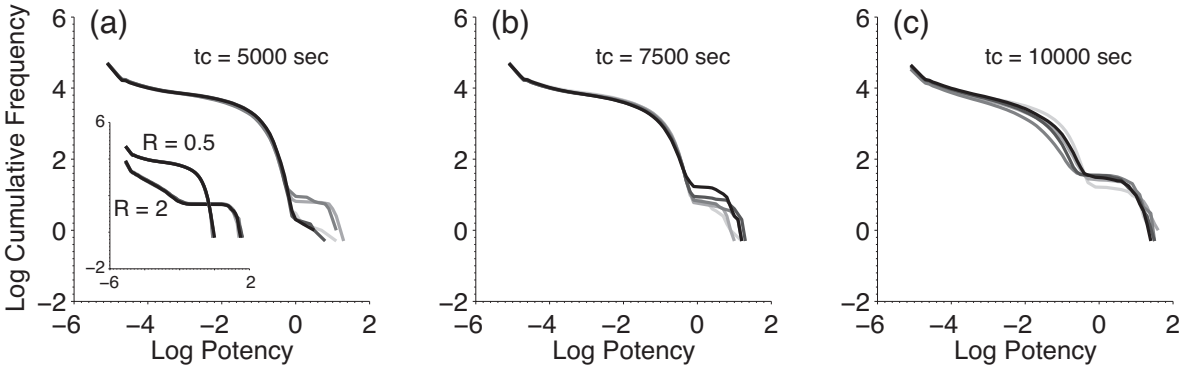

Figure 10. Evolution of temporal seismicity patterns for three systems with $b = 0.02$ discussed in Figure 8(b). Shown are the frequency-size distributions of five consecutive subcatalogs containing seismicity from two loading cycles ($2t^*$), covering the period between $t = 5t^*$ and $t = 15t^*$. The inset in (a) displays the (non) evolution of the frequency size distribution for models with fixed R (Fig. 3). Successively darker shades of grey indicate later time periods. The fluctuations suggest that extrapolations based on previous system dynamics possibly under or over estimate future earthquake occurrence.